Published by
NIGERIAN SOCIETY OF PHYSICAL SCIENCES
Available online @ https://journal.nsps.org.ng/index.php/jnsps

J. Nig. Soc. Phys. Sci. 8 (2026) 3180

Journal of the Nigerian Society of Physical Sciences

Dynamics of the Earth's magnetopause's subsolar location during solar cycle 24 in relation to the phases of geomagnetic storms of CME origin

Boukary Damiba, Christian Zoundi*, Abdoul Kader Segda

Laboratoire de Chimie Analytique, de Physique Spatiale et Energétique (L@CAPSE), Université Norbert ZONGO, Koudougou, Burkina Faso

Abstract

This article analyses the response of the subsolar position (R_o) of the Earth's magnetopause to geo-effective ICME storms in solar cycle 24, ranging from minor to extreme intensity, based on the model developed by Shue et al. (1998) and 1-minute OMNI data. The study combines a phase analysis of representative storms with an analysis of the influence of R_o variability on solar wind parameters, without phase distinction (correlations, time lags, Granger causality, and adjustments). The results show that the dynamics of R_o are driven almost exclusively by P_d in the minor and moderate storms studied, while a synergistic shift appears in strong and extreme storms, where magnetic reconnection or even magnetopause erosion becomes decisive. The crossing of the magnetopause at the subsolar point of the geosynchronous orbit (<6.6 R_e) is a signature of the main phase of the storm on 22 June 2015 (strong) and the initial and main phase of the storm on 17 March 2015 (extreme). The autocorrelation correction confirms the robustness of the high correlations observed. The relationships between R_o and P_d remain linear except for the extreme event, while B_z requires polynomial adjustments in most of the events studied. Variations in P_d and N precede those in R_o by 1 min to 3 min and significantly influence those in R_o, with a maximum effect at lag = 0 min in almost all events. The predominant response of R_o to the magnetic constraint imposed by B is delayed, with lag varying from 30 min to 7 min depending on the event, except in the extreme case where lag = 0 min, controlled by the structure of the magnetosphere, and B_z plays a secondary role except in the extreme case where it contributes to magnetic reconnection and magnetopause erosion.

DOI:10.46481/jnsps.2026.3180

Keywords: Magnetopause, Subsolar position, ICME storm, Empirical model, Solar wind

Article History :
Received: 16 October 2025
Received in revised form: 11 January 2026
Accepted for publication: 16 January 2026
Published: 28 February 2026

© 2026 The Author(s). Published by the Nigerian Society of Physical Sciences under the terms of the Creative Commons Attribution 4.0 International license. Further distribution of this work must maintain attribution to the author(s) and the published article's title, journal citation, and DOI.

Communicated by: B. J. Falaye

1. Introduction

The magnetopause is the essential dynamic interface of the Earth's magnetospheric system. It marks the boundary between the magnetosphere, which is governed by Earth's magnetic field, and the solar wind, a continuous stream of charged particles emitted by the Sun. Its position, particularly at the subsolar point, remains at a safe distance (R_o) and varies continuously in response to solar wind parameters and the interplanetary magnetic field (IMF). (R_o) is therefore a key indicator of magnetospheric compression and the vulnerability of space infrastructure.

*Corresponding author Tel. No: +226-7144-4242.
Email address: zounchr@yahoo.fr (Christian Zoundi)

Among the most disruptive solar structures, coronal mass ejections (CMEs) generate interplanetary shocks that can trigger intense geomagnetic storms. According to several studies [1–3], the most severe compressions of the magnetopause, especially during extreme storms, are driven by fast CMEs, which are often characterised by high density and an intense magnetic field.

Empirical and numerical models have been developed to explain these changes, and Refs. [4–6], propose a robust formulation that links R_o to the B_z component of the IMF and the solar wind dynamic pressure. Recent studies on the variation in the safety distance, such as Ref. [7], have highlighted time-lag and hysteresis effects, emphasising that the major R_o index depends not only on instantaneous conditions but also on the history of the solar wind. Additionally, Ref. [8] research on the long-term fluctuations of the magnetopause's subsolar location over five solar cycles has shown a significant reliance on specific solar wind parameters. Their approach, based on annual averages, confirmed the dominant role of these parameters in large-scale magnetospheric compression.

Nevertheless, a number of restrictions remain despite these developments. There are currently few continuous in situ observations of the magnetopause's dayside, and methods relying on stationary simulations or lengthy averages do not enable a precise distinction in R_o's response based on storm intensity or storm phase (initial, main, or recovery). Ref. [9] have also shown that transient phenomena such as ICMEs, particularly their ejecta, significantly impact the magnetopause dynamics through multiparametric interactions that still elude conventional models. This poses a significant problem for satellite operators, especially those whose control systems depend on the Earth's magnetic field to keep the satellite pointed in the right direction [10].

This is the setting for the current study, which aims to statistically analyse the dynamics of the Earth's magnetopause's subsolar location (R_o) in relation to the various stages of geomagnetic storms caused by CME shocks based on their intensity during solar cycle 24. The study employs an event-based, multiphasic methodology stratified by disturbance severity, using a representative sample of classified storms (minor, moderate, strong, extreme). It aims to evaluate the evolution of R_o during the initial, main, and recovery phases of each type of storm, to examine the correlations and time lags between R_o and the main parameters of the solar wind (P_d, B_z, B, N), to identify nonlinear relationships or delayed response effects of the magnetopause, and to compare the characteristic signatures of R_o according to CME event classes. The initial analysis focuses on a single representative case for each ICME storm category (minor, moderate, strong, and extreme), and this study extends it by adding two additional events of the same type. This approach aims to broaden the observational base, thereby strengthening the statistical validity of the results and enabling the identification of more reliable general trends in the relationships between the subsolar location R_o and solar wind parameters. On the other hand, for the category of extreme ICME storms, the analysis is based on a single event, this being the only case of an extreme ICME storm recorded during solar cycle 24, which gives it a special status in the study.

Table 1. Geomagnetic storm classification according to Ref. [12].

Category	Physical measurements
Descriptor	D_{ST} (nT)
Minor	-50 nT ≤ D_{ST} ≤ -30 nT
Moderate	-100 nT ≤ D_{ST} ≤ -50 nT
Strong	D_{ST} ≤ -100 nT
Extreme	D_{ST} ≤ -200 nT

By building on previous work, this study makes a targeted contribution to understanding magnetospheric compression mechanisms and aims to improve the modelling of Sun-magnetosphere interactions in a transient context, with direct implications for high-temporal-resolution space forecasting. The study's data and methodology are presented in section 2, followed by the results and discussion in section 3, and the conclusion in section 4.

2. Methodology

2.1. Different phases of a geomagnetic storm

Based on changes in geomagnetic indices, a geomagnetic storm can be divided into three phases. In equatorial regions and at low latitudes, these different phases can be observed through temporal variations in the D_{ST} (Disturbance storm time) index (see Figure 1).

1. An initial phase, which is a brief transient phase (a few hours) during which the solar wind compresses the magnetosphere. It results in an increase in D_{ST} and a sudden increase in the Chapman-Ferraro current at the magnetopause and in the horizontal component H of the Earth's magnetic field;
2. A main phase, during which the magnetosphere remains compressed. This phase lasts from a few hours to a day. It is characterised by a drop in D_{ST}, caused by the intensification of the ring current, and by a slight decrease in the H component of the Earth's magnetic field;
3. A recovery or restoration phase, during which the disturbances decrease more or less rapidly, leading to a gradual increase in the D_{ST} and the magnetosphere returns to its normal size. Its duration ranges from a day to several days.

2.2. Different classes of geomagnetic storms

Geomagnetic storms are classified according to their intensity or degree of disturbance using magnetic indices that reflect geomagnetic activity. For example, we have the D_{ST} index in the mid and low latitudes of the magnetic equator with a temporal resolution of one (01) hour, the symmetric disturbance index of the horizontal component (H) of the Earth's magnetic field (SYM-H) with a temporal resolution of one (01) minute [11]. The D_{ST} index was used according to the classification proposed by Ref. [12]. This classification is shown in Table 1.

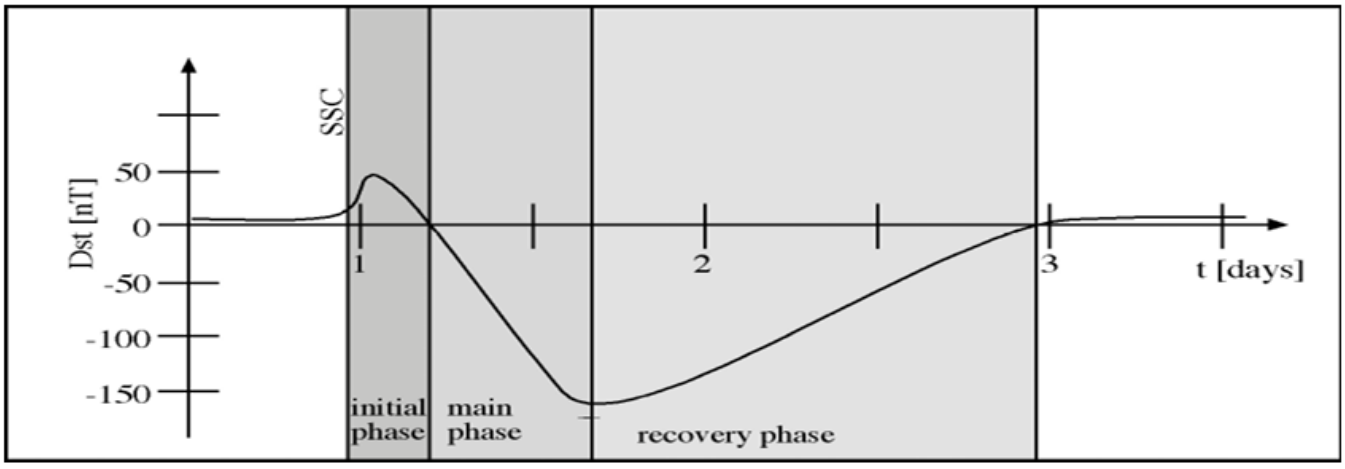

Figure 1. Different phases of a geomagnetic storm.

Table 2. Geomagnetic storms caused by CMEs selected for the study.

Storm class	Storm date	CME type	Emission (UTC)	Angle	Impact (UTC)	$D_{ST,\min}$ (nT)	Start	End
Minor	21-04-2014	Partial halo	15-04-2014 (18:24:05)	360	20-04-2014 (10:21:00)	-32	21-04-2014 (07:30:00)	22-04-2014 (07:48:00)
	05-06-2011	Partial halo	01-06-2011 (18:36:06)	186	04-06-2011 (20:45:00)	-47	05-06-2011 (02:00:00)	05-06-2011 (19:00:00)
	09-03-2018	Partial halo	06-03-2018 (01:25:41)	136	09-03-2018 (18:09:00)	-39	09-03-2018 (22:00:00)	11-03-2018 (00:00:00)
Moderate	04-08-2010	Halo	01-08-2010 (13:42:05)	360	03-08-2010 (17:01:34)	-74	04-08-2010 (09:54:00)	05-08-2010 (00:56:15)
	02-10-2013	Halo	29-09-2013 (22:12:05)	360	02-10-2013 (01:54:00)	-72	02-10-2013 (23:00:00)	03-10-2013 (22:00:00)
	06-11-2015	Partial halo	01-11-2015 (23:24:04)	171	06-11-2015 (18:18:00)	-87	07-11-2015 (06:00:00)	08-11-2015 (16:00:00)
Strong	23-06-2015	Halo	19-06-2015 (06:42:50)	360	22-06-2015 (05:08:34)	-198	23-06-2015 (01:36:25)	24-06-2015 (13:10:42)
	24-10-2011	Halo	22-10-2011 (01:25:53)	360	24-10-2011 (18:31:00)	-147	24-10-2011 (22:00:00)	25-10-2011 (16:00:00)
	14-07-2012	Halo	11-07-2012 (01:25:27)	360	14-07-2012 (18:09:00)	-139	15-07-2012 (06:00:00)	17-07-2012 (05:00:00)
Extreme	17-03-2015	Halo	15-03-2015 (01:48:05)	360	17-03-2015 (04:00:00)	-234	17-03-2015 (13:08:34)	18-03-2015 (23:21:25)

Note: Source: List of CMEs (Richardson and Cane).

The geomagnetic storm events induced by CMEs selected for this study are recorded in Table 2. These events are all located in solar cycle 24 (2008-2018).

2.3. Data analysis methods

Our estimate of the subsolar distance of the Earth's magnetopause, also known as the safety distance, is based on the empirical model developed by Ref. [4] and improved in 1998. This model is widely used in the scientific community for its ability to represent the shape and location of the magnetopause as a function of solar wind conditions and the interplanetary magnetic field (IMF). It is based on a parametric equation that describes the magnetopause geometry as a function of the solar zenith angle, with two key parameters: R_o, which represents the subsolar distance, and α, which controls the degree of flaring of the magnetospheric tail.

The 1998 version introduces a more flexible, physically consistent formulation that accounts for the nonlinearity of the B_z field and the dynamic pressure P_d. It improves the continuity between positive and negative B_z regimes, thereby allowing a better representation of magnetopause variations across various contexts [5]. The model is appreciated for its simplicity,

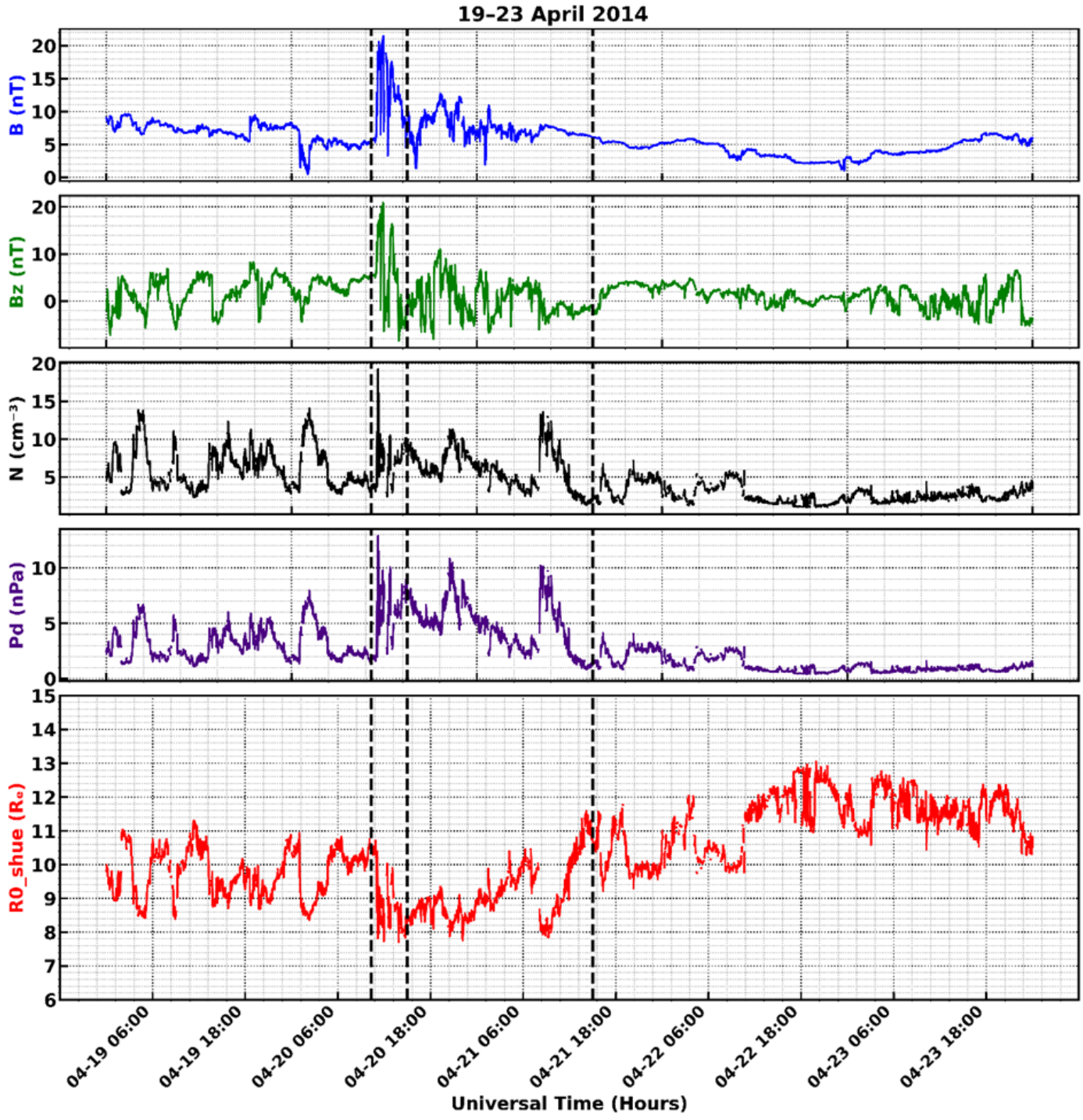

Figure 2. From top to bottom, daily variations in IMF intensity (B), north–south component of IMF (B_z), proton density (N), solar wind dynamic pressure (P_d), and subsolar location R_0 of the magnetopause during the minor storm from April 19 to 23, 2014.

robustness, and compatibility with in situ observations, particularly those from space missions that primarily operate at the equatorial plane and low latitudes, such as THEMIS and MMS. The model is also nominally suitable for predicting extreme solar wind conditions that can lead to large deformations of the magnetopause [5], as confirmed by Ref. [9]. This model has been widely used as a reference in previous work.

In this study, the formula for the subsolar location of the magnetopause used is represented by the equation (1):

$$R_o = (10.22 + 1.29 \tanh[0.184(B_z + 8.14)])(P_d)^{-\frac{1}{6.6}}, \quad (1)$$

where R_o represents the location of the subsolar point of the Earth's magnetopause estimated in Earth radius (R_e), B_z denotes the (north-south) component of the interplanetary mag-

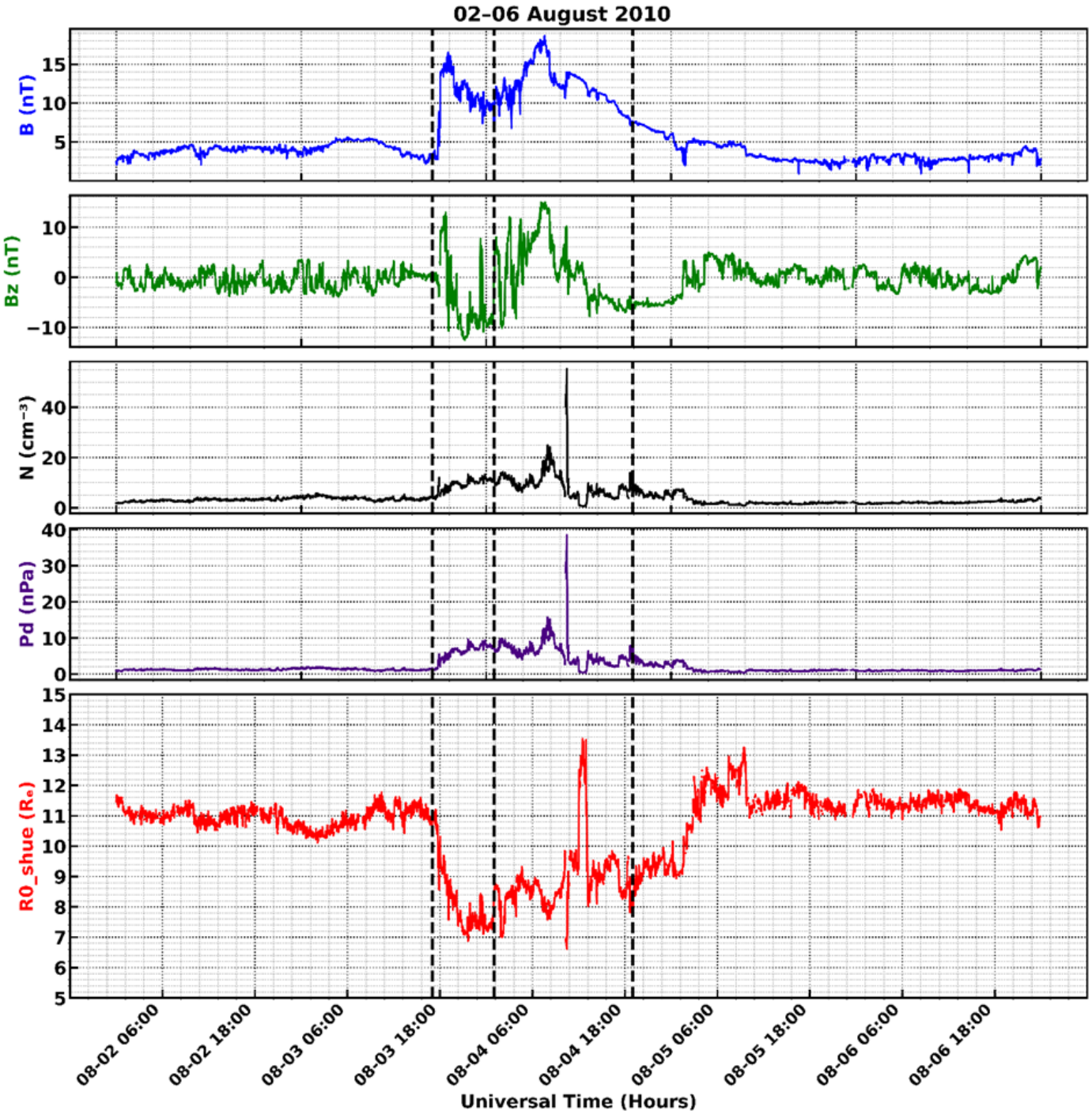

Figure 3. From top to bottom, daily variations in IMF intensity (B), north–south component of IMF (B_z), proton density (N), solar wind dynamic pressure (P_d), and subsolar position R_0 of the magnetopause during the moderate storm from August 2 to 6, 2010.

netic field (IMF) in (nT), and P_d the dynamic pressure of the solar wind in (nPa).

2.4. *Methodological approach: methods for processing time series, statistical validation, causality tests and uncertainty assessment*

Correlations between R_o and solar parameters (P_d, B, B_z, N) were assessed, accounting for autocorrelation in the time series. Statistical significance and confidence intervals were adjusted using the effective number of degrees of freedom (Neff), estimated according to the method of Ref. [13], to limit the overestimation of confidence levels due to temporal redundancy in observations.

Directional temporal relationships were examined using Granger causality tests. The stationarity of the series was verified using the augmented Dickey–Fuller (ADF) test [14], and

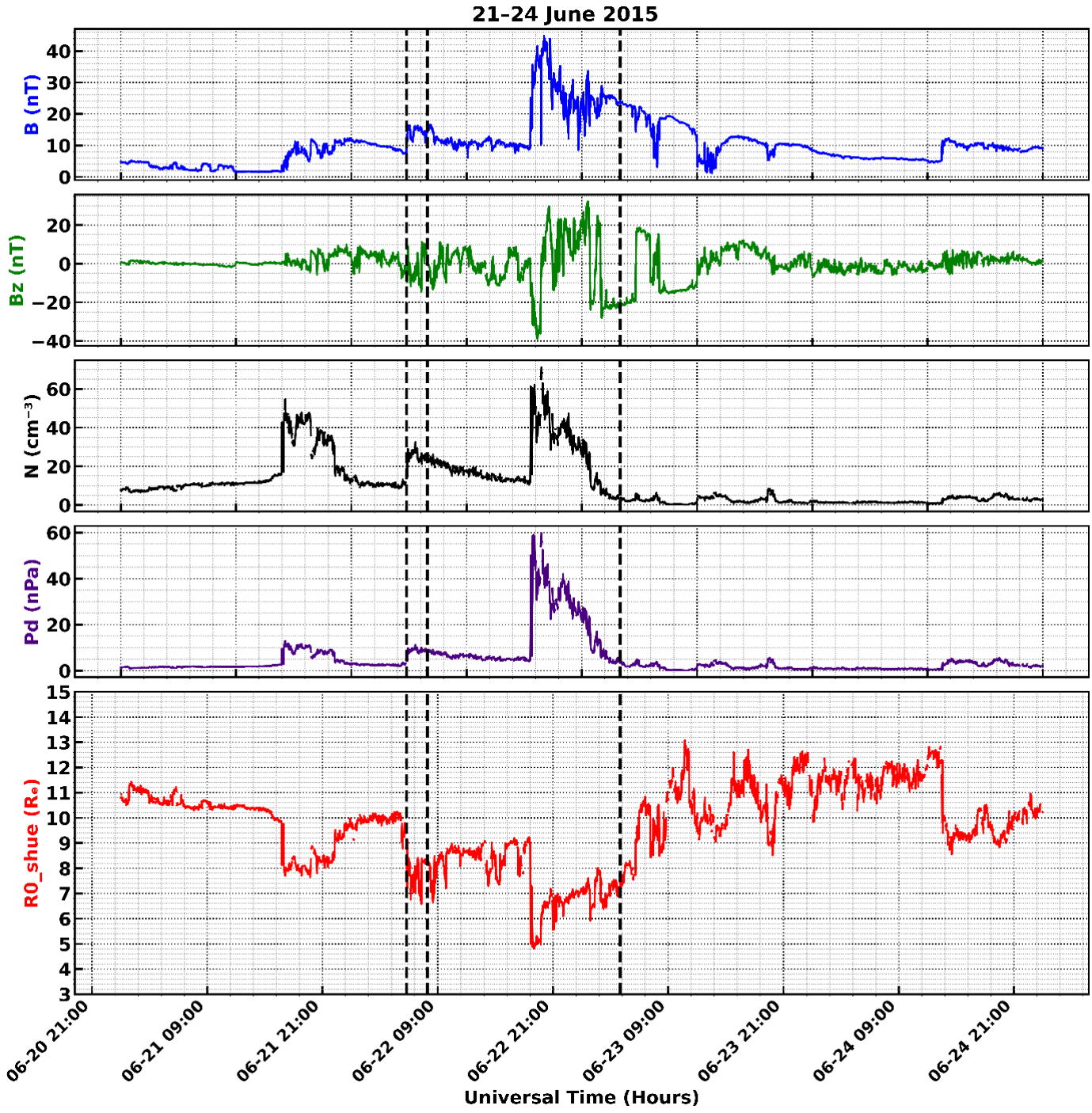

Figure 4. From top to bottom, daily variations in IMF intensity (B), north–south component of IMF (B_z), proton density (N), solar wind dynamic pressure (P_d), and subsolar position R_0 of the magnetopause during the phases of the severe storm from June 21 to 24, 2015.

non-stationary series were made stationary by differentiation where necessary. Causality tests were performed in a multiple lag autoregressive framework, with significance assessed using F-tests in accordance with Granger's original formulation [15] and subsequent developments in VAR analysis. Granger causality is a commonly used approach in space geophysics and space weather studies for analysing causal relationships between geophysical parameters (e.g., Ref. [16]).

The uncertainty associated with causal lags was estimated using a stationary bootstrap, which reproduces the temporal dependence of the series during resampling without assuming independence among observations [17]. This approach was used to construct empirical distributions of dominant lags and assess their statistical stability in a context of temporal dependence and potential non-normality [18]. Finally, linear and second-degree polynomial regression models were explored in a uni-

variate setting, with cross-validation respecting the temporal order of the data.

3. Results and discussions

This section will first focus on variations in the subsolar position R_o of the magnetopause throughout geomagnetic storms, then on correlation analysis and linear and non-linear regression between the subsolar position R_o of the Earth's magnetopause and solar wind parameters during geomagnetic storms, and finally on Granger causality analysis, cross-correlation and time lag between the subsolar position of the Earth's magnetopause and solar wind parameters.

3.1. Variation of the subsolar location of the magnetopause during the entire course of the minor storm of April 21, 2014

The graphs in Figure 2 below show the different subsolar locations of the Earth's magnetopause under the influence of solar wind parameters and the interplanetary magnetic field (IMF) during the minor CME storm that occurred on April 20, 2014. The observation of Figure 2 shows a marked variability for R_o in direct response to fluctuations in solar wind parameters and the interplanetary magnetic field IMF.

The first vertical line indicates the time of the shock. Before this first line, we have the pre-storm (calm) period; between the first and second vertical lines, the initial phase of the minor storm; between the second and third vertical lines, its main phase; and after the third vertical line, its recovery phase.

Pre-storm phase: Before the impact of the coronal mass ejection (CME), between 19 April and 20 April (until 10:20 UT), the subsolar position (R_o) of the Earth's magnetopause showed remarkable stability, oscillating slightly between 9.5 R_e and 11 R_e. As shown by Refs. [4, 19, 20], the subsolar point is, on average, located at about 10 R_e (Earth radii) under normal solar conditions. This configuration reflects a quasi-static state of equilibrium. This principle, introduced by Ref. [21] and further developed by Ref. [22], is based on the fact that the shape and position of the day boundary continuously adjust to maintain equilibrium between the pressure of incident solar plasma and the internal magnetic pressure of the magnetosphere. Here, the magnetic resistance precisely compensates for a moderate dynamic pressure (P_d) (3 nPa to 5 nPa). The absence of dominant polarity in the interplanetary magnetic field (B_z) prevents erosion by reconnection, thereby validating the application of reference models for standard solar conditions.

The quasi-steady state was abruptly disrupted at 10:21 UT on 20 April by the impact of the CME shock. A sudden compression of the boundary was observed, resulting in a 1.3 reduction and propelling the subsolar point to a minimum of 7.9 R_e. This dynamic was driven by an increase in dynamic pressure P_d by an order of magnitude (a factor of 4-5), reaching values exceeding 14 nPa. In accordance with the conclusions of Ref. [23], this response is the direct signature of a supersonic shock. Since the B_z component remains close to zero, the compression here is purely mechanical, with the inward displacement being strictly correlated with the increase in density and intensity of the total interplanetary magnetic field (B > 20 nT).

Initial phase: between 10:21 UT and 15:00 UT on 20 April 2014, the magnetopause was maintained under variable compression, with R_o fluctuating between 7.9 R_e and 9.9 R_e. This instability is driven by residual P_d pulses (3.4 nPa to 10 nPa).

During the main phase (from 20 April at 15:00 UT to 21 April at 15:00 UT), the magnetopause maintains a similar dynamic to that observed in the initial phase. Despite the storm's overall evolution, variations in R_o remain closely correlated with low-amplitude fluctuations in dynamic pressure Pd. This observation indicates that, for this specific event, direct control by the solar wind prevails over internal magnetic coupling processes.

Recovery phase: from 21 April after 15:00 UT, the system begins a gradual relaxation phase. The subsolar position R_o stabilises at distant values between 10 R_e and 12.8 R_e, reflecting a state of maximum relaxation of the magnetopause. This return to the nominal configuration is correlated with a drastic drop in P_d to very low values (1.5 nPa to 2 nPa). The restoration of interplanetary calm allows the pressure balance between the solar wind and Earth's magnetic pressure at the magnetopause to be restored, returning the latter to its initial spatial configuration and marking the end of the CME's influence.

3.2. Variation of the subsolar location R0 of the magnetopause during the entire course of the moderate storm of August 4, 2010

During the moderate geomagnetic storm of August 4, 2010, the subsolar location R_o of the Earth's magnetopause showed pronounced variability in response to the strong fluctuations in the solar wind induced by the arrival of a coronal mass ejection (CME) (Figure 3).

The first vertical line indicates the time of the shock. Before this first line, we have the pre-storm (calm) period; between the first and second vertical lines, the initial phase of the moderate storm; between the second and third vertical lines, its main phase; and after the third vertical line, its recovery phase.

Pre-storm phase: between 2 and 3 August (until 17:00 UT), the magnetopause is in a state of relaxation characteristic of periods of interplanetary calm. The subsolar position (R_o) oscillates steadily between 10.5 R_e and 11.5 R_e. This configuration is maintained by minimal dynamic pressure (P_d) (~1 nPa) and a near-zero B_z component ($B_z \approx 0$ nT). This interval defines the reference state required for quantifying the dynamic disturbances induced by the arrival of the solar structure.

Initial phase: an abrupt change in conditions occurred on 3 August at 17:40 UT, marking the impact of the CME shock front. An increase in dynamic pressure (P_d) of one (01) order of magnitude was observed, rising from 1 nPa to 10 nPa in a matter of minutes. This peak in P_d compresses the magnetopause, reducing R_o by a factor of 1.6 to a minimum of 7 R_e (observed around 22:00 UT). Analysis shows that the compression observed is not exclusively mechanical in origin. The southward tilt of the B_z component introduces a secondary magnetic contribution, in agreement with the work of Ref. [24], who showed

that a southward orientation of the interplanetary magnetic field favours the approach of the magnetopause from a state of pressure equilibrium. In this moderate regime, the southward orientation of B_z does not lead to fully developed erosion of the magnetosphere on the day side, but activates an incipient magnetic coupling. As described by Refs. [25–27], this coupling is accompanied by the activation of region 1 currents, which partially weaken the magnetic field on the day side. This relaxation reduces the magnetosphere's ability to resist the dynamic pressure of the solar wind, allowing the latter to dominate more effectively and accentuate the compression of the magnetopause, without exceeding the limits of a regime in which the compression of the magnetopause remains essentially governed by the dynamic pressure of the solar wind, with the magnetic contribution playing a secondary role.

The main phase, between 01:00 UT and 19:00 UT on 4 August, shows a complex dynamic signature, alternating between residual compression and major expansion. The highlight of this phase is a spectacular expansion of the magnetopause reaching 13.5 R_e between 12:00 UT and 13:00 UT. This phenomenon, representing a growth of nearly 90% from the minimum of the initial phase, resulted from a drastic drop in P_d (falling to 0.5 nPa) coupled with a sustained shift of B_z towards the north. This 'rebound' observed in this event is characteristic of moderate storms where the rarefaction of solar plasma following the dense front of the CME allows for an exceptional relaxation of the magnetospheric cavity, a behaviour documented by Refs. [1, 2].

Recovery phase: from 19:00 UT on 4 August, the system began recovery. The subsolar position (R_o) stabilised at distant values (11 R_e to 13 R_e), reflecting a state of maximum relaxation of the magnetospheric cavity. The return of solar wind parameters to their reference levels (~1 nPa for P_d and ~1 cm^{-3} for density N) confirms that the magnetosphere is free from the compressive stresses imposed by the CME. The dissipation of major fluctuations marks the restoration of Chapman-Ferraro equilibrium under nominal post-storm conditions.

3.3. *Variation of the subsolar location R_o of the magnetopause during the entire course of the intense storm of June 23, 2015*

During the strong geomagnetic storm of June 23, 2015, the subsolar location of the Earth's magnetopause R_o (Figure 4) experienced particularly strong and rapid fluctuations in response to extreme changes in solar wind conditions induced by the arrival of a coronal mass ejection (CME). We analyse the variability of R_o during this event.

The first vertical line indicates the time of the shock. Before this first line, we have the pre-storm (calm) period; between the first and second vertical lines, the initial phase of the severe storm; between the second and third vertical lines, its main phase; and after the third vertical line, its recovery phase.

Pre-storm phase: the period before 05:44 UT on 22 June. At the start of this phase, the magnetosphere was initially calm, with the subsolar position (R_o) stabilised between 10 R_e and 11 R_e. However, an isolated compression was observed at 17:00 UT on 21 June, bringing R_o back to 8 Re. Although no interplanetary coronal mass ejection (ICME) events are listed in the official catalogues for this interval, the simultaneous increase in dynamic pressure (P_d) and magnetic field intensity (B) suggests the impact of an unidentified plasma cloud structure. This forcing, lasting approximately eight (08) hours, appears to play a role in preconditioning the magnetospheric cavity before the arrival of the main shock.

Initial phase: the CME shock front impacts at 05:44 UT on 22 June, causing a sudden compression of the magnetopause. The subsolar position (R_o) decreases by a factor of 1.5, reaching a minimum of 6.8 R_e. This response is driven by a Pd pulse reaching 10 nPa, associated with a plasma density N>25 cm^{-3}. During this phase, the B_z component exhibits rapid fluctuations around 0 nT, with intermittent excursions to positive and negative values, without remaining in any particular range for long. Under these conditions, the influence of B_z on the magnetopause is intermittent and unstable: periods of $B_z < 0$ temporarily promote erosion and compression, while passages of $B_z > 0$ allow partial relaxation, preventing sustained displacement of the magnetopause. This indicates that in this initial phase, the sustained inward displacement of the magnetopause results from a dominance of purely mechanical forcing mechanisms. This observation validates the momentum transfer results of Ref. [23] under conditions of negligible magnetic reconnection.

Main phase: The main phase, which began at 08:00 UT on 22 June, was characterised by impulsive dynamics. After a brief expansion to 9 R_e following a northward orientation of B_z, the system interacted with the compressive region of the ICME between 18:00 UT and 20:00 UT. The magnetopause then undergoes marked compression, with R_o reaching a minimum of 5 R_e, placing the subsolar point well below the geosynchronous orbit (6.6 R_e). This compression results from the combined action of two fundamental mechanisms: the first mechanism is a dramatic increase in the dynamic pressure of the solar wind (P_d~49 nPa) associated with a high solar wind density (approximately 58 cm^{-3}): the solar wind exerts a direct force on the magnetopause, pushing the Earth's magnetic field lines inward. According to the pressure equilibrium, such an increase in P_d moves the magnetopause much closer to Earth than under normal conditions. The second mechanism is the strong southward orientation of B_z (around −40 nT) concomitant with an intensification of the interplanetary magnetic field B, which becomes more intense (45 nT): this configuration promotes magnetic reconnection on the day side of the Earth's magnetopause, allowing solar plasma flux to temporarily enter the magnetosphere. The reconnection opens up Earth's magnetic field lines and promotes the magnetopause's approach towards Earth, which amplifies the compression induced by the dynamic pressure of the solar wind in a very short time during this main phase, which lasted only about two (02) hours, in accordance with the mechanisms described by Refs. [24, 27]. Our results in this main phase of a strong geomagnetic storm induced by ICME demonstrate that a strong pulse of P_d, or a strong pulse of P_d combined with a strong rotation of B_z from north to south, or a strong rotation of B_z from north to south without a pulse, is sufficient to

bring the magnetopause inside the geosynchronous orbit.

Finally, during the recovery phase, after 04:00 UT, R_o gradually rose above 8 R_e, indicating a relaxation of solar wind pressure and a B_z oscillating around 0 nT, also indicating a gradual return to normal conditions.

Our results during the main phase of the geomagnetic storm of 22 June 2015, based on the model by Ref. [5], are consistent with the observations of Ref. [28], which identify magnetopause crossings by the GOES 13 and GOES 15 satellites between 18:30 UT and 20:00 UT on 22 June 2015, caused by a similar increase in density (10 cm^{-3} to 60 cm^{-3}) and a southward orientation of B_z reaching -40 nT. Both studies confirm that the magnetopause moved inside the geosynchronous orbit before relaxing following a northward rotation of B_z and a decrease in density. Our results provide further clarification by distinguishing three scenarios for the passage of the magnetopause below the geosynchronous orbit: a single pulse of P_d, a pulse combined with a southward rotation of B_z, or a southward rotation of B_z without a dynamic pressure pulse, thus highlighting the complexity of the interactions between solar wind parameters and magnetospheric dynamics for this case of a CME-induced geomagnetic storm.

3.4. Variation of the subsolar location R0 of the magnetopause during the entire course of the extreme storm of March 17, 2015

The extreme geomagnetic storm of March 17, 2015, often referred to as the "Saint Patrick's Day Storm," is an example of extreme interaction between a coronal mass ejection (CME) and the Earth's magnetosphere during solar cycle 24. The evolution of the subsolar magnetopause location, R_o (Figure 5), during this event shows strong fluctuations in the boundary layer.

The first vertical line indicates the time of the shock. Before this first vertical line, we have the pre-storm (calm) period; between the first and second vertical lines, the initial phase of the extreme storm; between the second and third vertical lines, its main phase; and after the third vertical line, its recovery phase.

The pre-storm phase lasted from 16 to 17 March at around 04:45 UT. It was characterised by unstable magnetopause dynamics, with the subsolar position fluctuating upstream of the initial phase between 7.4 R_e and 10 R_e. In fact, as early as 02:00 UT on 16 March, a marked compression reduces R_o to 7.4 R_e. This magnetopause dynamics is a direct response to high dynamic pressure P_d (>12 nPa) associated with high solar wind plasma density ($N \approx 40$ cm^{-3}). This 'breathing' phase of the magnetopause reflects the heterogeneity of the precursor solar wind. The role of the magnetic component B_z is decisive here: a strongly negative orientation between 02:00 UT and 06:00 UT intensifies reconnection, preventing the system from stabilising at its nominal position. It was only after 04:00 UT on 17 March that the return to a north polarity of B_z and a drop in dynamic pressure P_d allowed a transient relaxation to 9.8 R_e.

Initial phase: the arrival of the ICME shock wave after 04:30 UT triggers a strong compression of the Earth's magnetopause. The subsolar position R_o decreases by 3.6 R_e (from 9.5 R_e to 5.9 R_e), crossing the geosynchronous orbit (6.6 R_e). This response, consistent with the models of Ref. [23], illustrates the impact of a supersonic shock, with dynamic pressure reaching extreme levels (30 nPa) and plasma density close to 40 cm^{-3}. The simultaneous increase in the total magnetic field (B) and the southward tilt of B_z suggest that, from the initial impact, the magnetopause is subjected to a double constraint: violent mechanical compression and magnetic reconnection, which erode the nascent magnetopause.

During the main phase, from 17 March at 08:00 UT to approximately 23:00 UT, R_o values fluctuated between approximately 8 R_e and 5.2 R_e. The lowest values were recorded at 14:00 UT and 17:00 UT, indicating extreme compression of the magnetosphere. This compression was caused by a sudden increase in P_d from around 30 nPa to 39 nPa linked to high solar wind density (58 cm^{-3}) and a significant southward rotation of B_z (up to -20 nnT) over a prolonged period. During this time, the dynamic pressure P_d remained high, allowing magnetopause erosion to set in, making it even more vulnerable at the subsolar point.

This erosion process, well documented in the literature Refs. [24, 29], occurs when the interplanetary magnetic field (IMF) is oriented southward, facilitating magnetic reconnection on the day side. This reconnection creates open field lines that are transported towards the magnetotail, reducing the magnetic flux on the day side. When the rate of reconnection on the day side exceeds that on the night side, the magnetopause moves towards Earth. This mechanism is corroborated by statistical observations [4, 27, 30] and numerical simulations [31]. Thus, our results confirm that the prolonged stability of B_z in the south, under strong dynamic pressure, is a key factor in the erosion of the magnetopause and its extreme approach to Earth during an extreme geomagnetic storm induced by an ICME.

During this extreme geomagnetic storm caused by an ICME, the magnetopause at the subsolar point, as modelled by Ref. [5], was compressed beyond the geosynchronous orbit in both the initial and main phases. Unlike the strong storm studied, the intensity of the ICME disturbance is more pronounced only during the main phase, with the magnetopause at the subsolar point moving inside the geosynchronous orbit. It should be noted that these significant compressions can cause the magnetopause to cross the drift shells (magnetopause shadowing). This phenomenon is the main process responsible for rapid particle losses in the outer belt above 100 keV [32].

During the recovery phase, after 23:00 UT on 17 March, all solar wind parameters and B intensity dropped to low values, B_z oscillated around 0 nT, and R_o oscillated between 10 and 9 R_e, indicating that the magnetopause had been released from the constraints imposed by ICME, signalling its stabilisation.

Our results from the main phase of this extreme ICME-induced storm are consistent with those of Ref. [33], who used multi-mission data to identify an intensification of field-aligned currents, an equatorial shift of the auroral oval, and magnetopause crossings, confirming the global impact of reconnection on the day side of the magnetosphere.

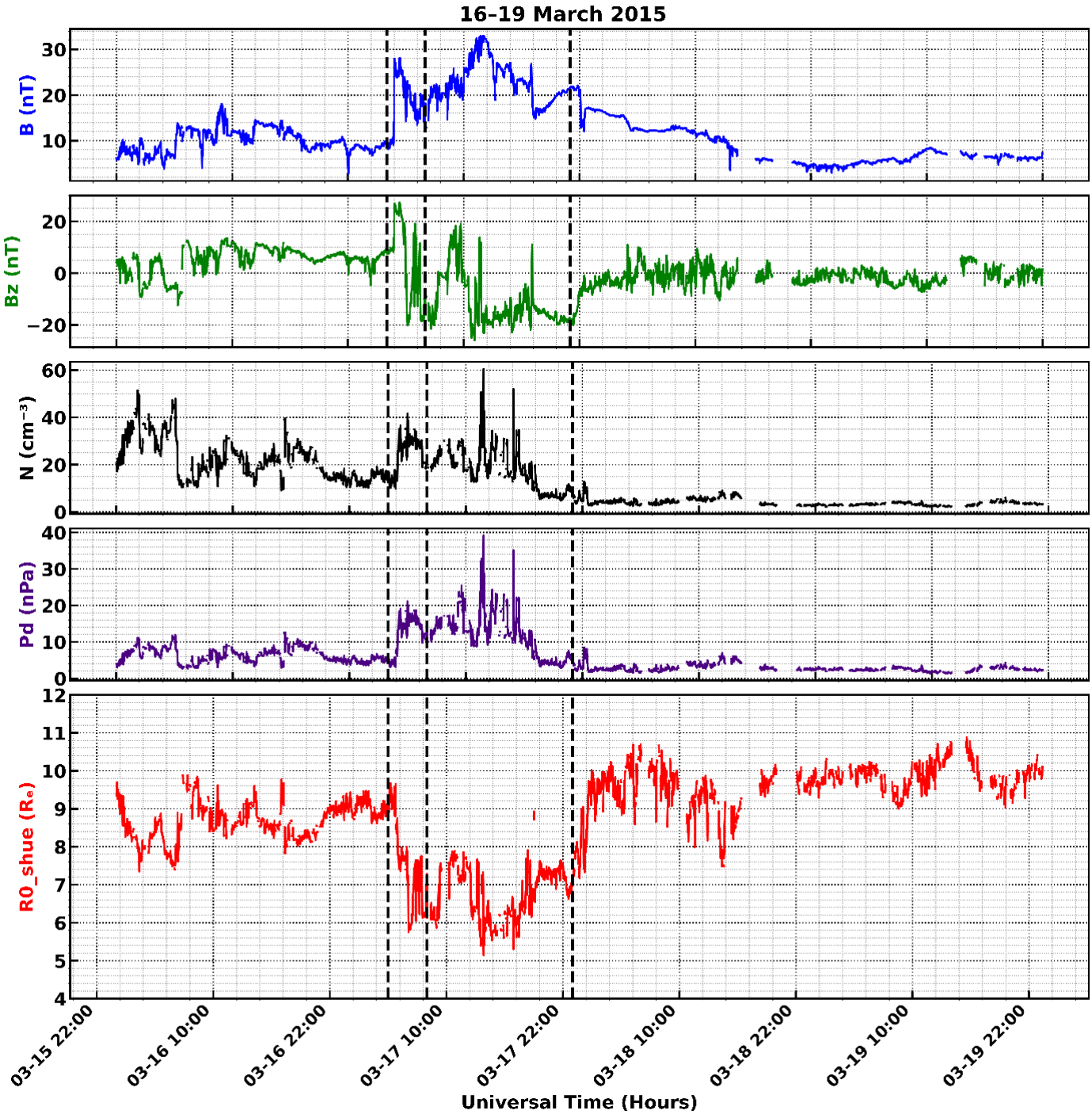

Figure 5. From top to bottom, daily variations in IMF intensity (B), north–south component of IMF (B_z), proton density (N), solar wind dynamic pressure (P_d), and subsolar position R_0 of the magnetopause during the extreme storm from March 16 to 19, 2015.

Table 3. Indicators of statistical robustness and model fidelity (linear and polynomial) of the influence of solar wind parameters on R_o during the complete evolution of the moderate ICME storm of 4 August 2010.

Parameters	Neff	r	IC95%	p-value	RMSE Lin ($\pm\sigma$)	RMSE Poly2 ($\pm\sigma$)
(P_d, R_o)	77.3	-0.91	[-0.94, -0.86]	0	0.59 ± 0.26	0.35 ± 0.16
(B_z, R_o)	116.4	-0.01	[-0.19, 0.18]	0.946	1.40 ± 0.45	1.34 ± 0.47
(B, R_o)	78.3	-0.58	[-0.71, -0.41]	2.15×10^{-8}	1.28 ± 0.23	1.92 ± 1.28
(N, R_o)	81.9	-0.89	[-0.93, -0.83]	0	0.68 ± 0.26	0.49 ± 0.20

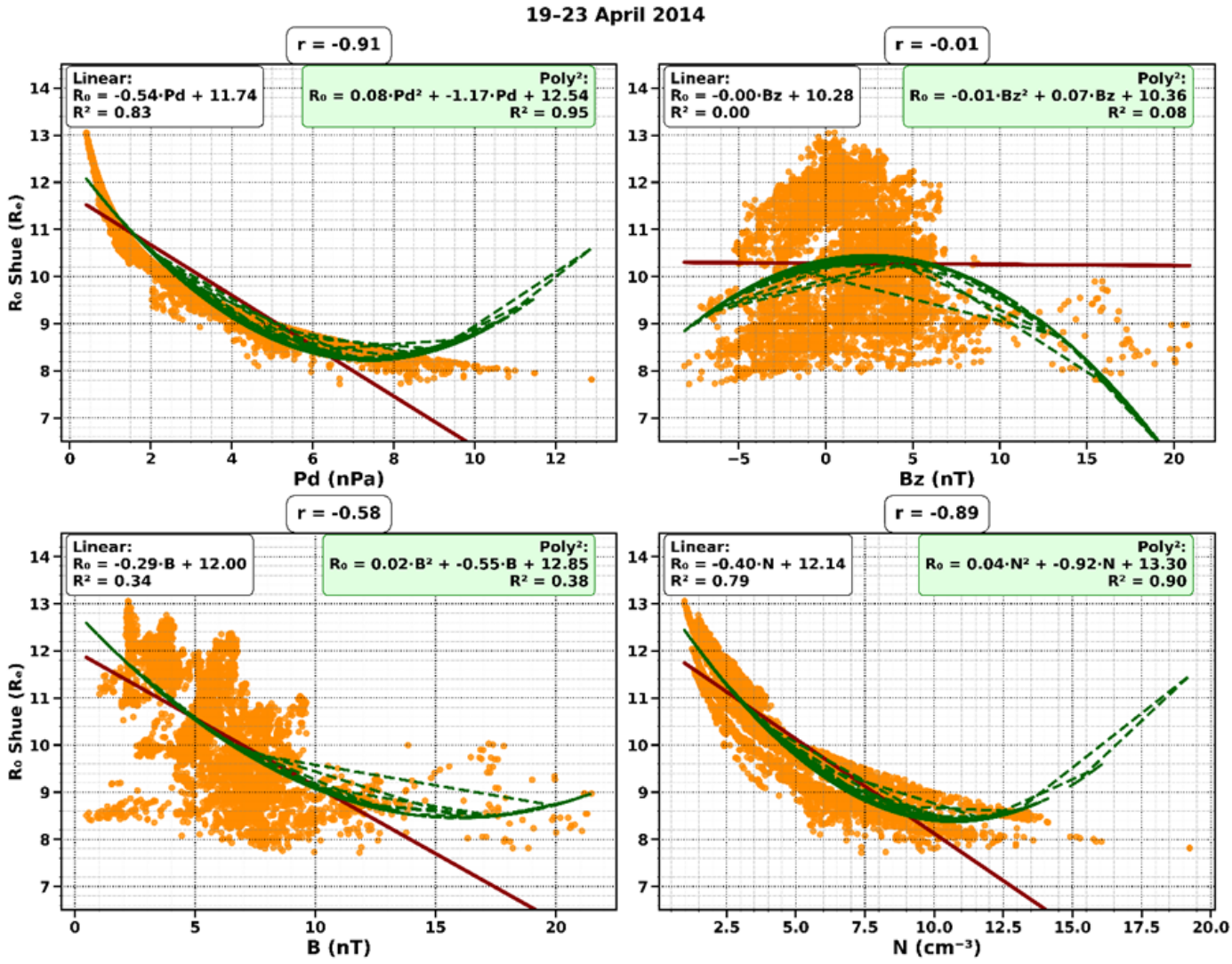

Figure 6. Linear and nonlinear correlation and regression between the subsolar location R_0 of the Earth's magnetopause and P_d, B_z, B, and N during the entire evolution of the minor storm on April 20, 2014.

Table 4. Correlation and regression coefficient values between R_o and solar wind parameters during moderate CMEs 2 (2 October 2013) and 3 (6 November 2015).

Events	Minor Storm 2			Minor Storm 3		
Indicators of dependency	Corr(r)	Linear (R^2)	Poly^2 (R^2)	Corr(r)	Linear (R^2)	Poly^2 (R^2)
(R_o, P_d)	-0.89	0.79	0.91	-0.88	0.77	0.88
(R_o, N)	-0.87	0.75	0.86	-0.85	0.72	0.76
(R_o, B)	-0.76	0.58	0.61	-0.35	0.12	0.19
(R_o, B_z)	-0.11	0.01	0.22	0.04	0.00	0.10

3.5. *Correlation analysis and linear and nonlinear regression between the subsolar location R_o of the Earth's magnetopause and solar wind parameters during geomagnetic storms*

To complement the analysis of temporal variability in R_o, this section focuses on the quantitative evaluation of the relationships between R_o and solar wind parameters across categories of geomagnetic storms induced by coronal mass ejections (CMEs).

Table 5. Indicators of statistical robustness and model fidelity (linear and polynomial) of the influence of solar wind parameters on R_o during the complete evolution of moderate storms ICME 2 (02-10-2013) and 3 (06-11-2015).

Events	Parameters	Neff	r	IC95%	p-value	RMSE Lin ($\pm\sigma$)	RMSE Poly2 ($\pm\sigma$)
Minor Storm 2	(P_d, R_o)	44.9	-0.89	[-0.94, -0.80]	6.66×10^{-16}	1.82 ± 2.30	14.08 ± 27.22
	(B_z, R_o)	58.7	-0.11	[-0.36, 0.15]	0.405	1.49 ± 0.81	1.34 ± 0.73
	(B, R_o)	40.6	-0.76	[-0.87, -0.59]	1.08×10^{-8}	1.45 ± 1.16	14.36 ± 26.88
	(N, R_o)	45.2	-0.87	[-0.93, -0.77]	1.04×10^{-14}	0.82 ± 0.38	1.00 ± 0.80
Minor Storm 3	(P_d, R_o)	64.4	-0.88	[-0.92, -0.81]	0	0.44 ± 0.22	0.35 ± 0.22
	(B_z, R_o)	72.8	0.04	[-0.19, 0.27]	0.724	0.87 ± 0.28	0.84 ± 0.26
	(B, R_o)	58.8	-0.35	[-0.56, -0.10]	6.80×10^{-3}	0.86 ± 0.27	2.44 ± 3.42
	(N, R_o)	64.9	-0.85	[-0.90, -0.76]	0	0.48 ± 0.26	0.44 ± 0.30

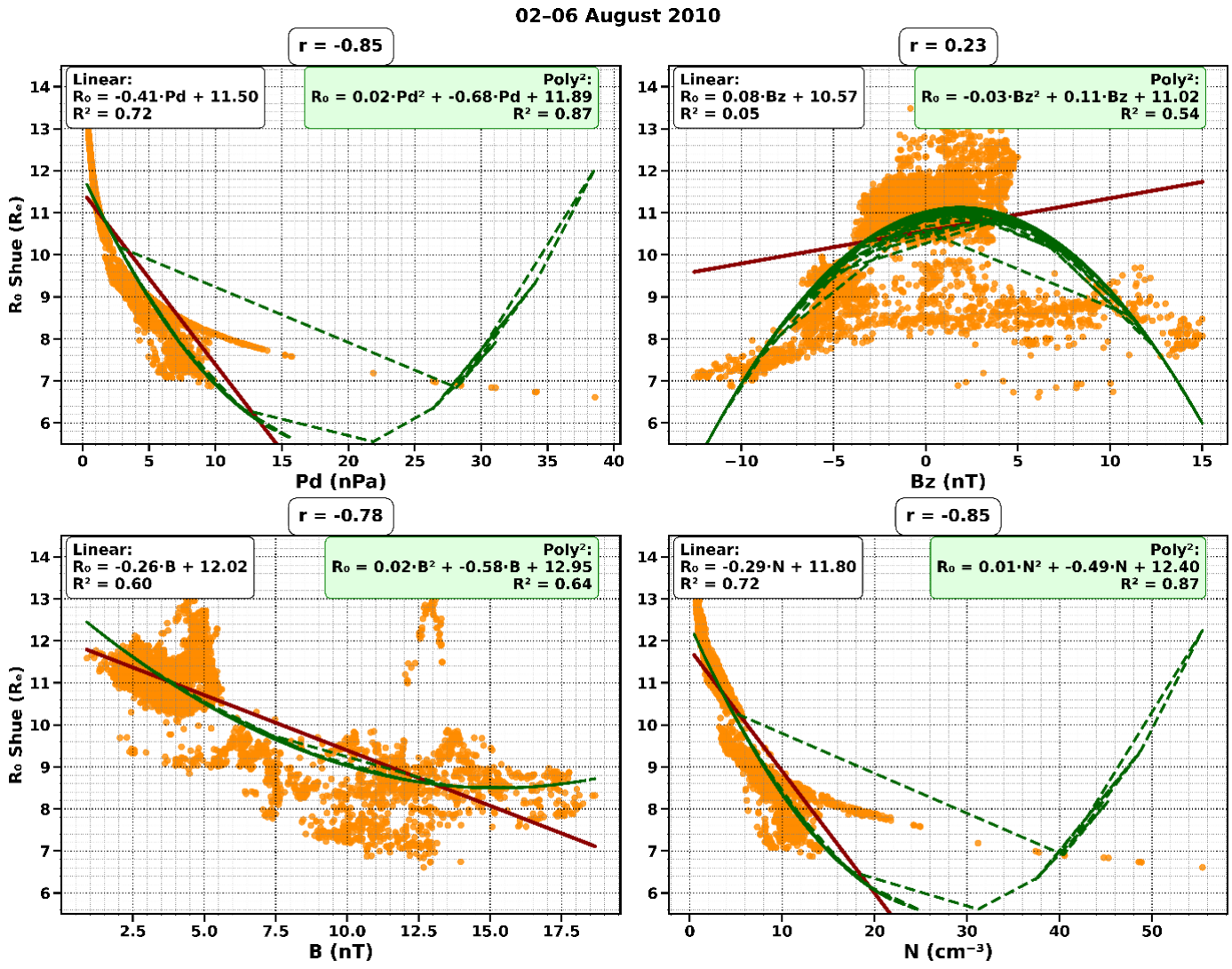

Figure 7. Correlation and linear and nonlinear regression between the subsolar location R_o of the Earth's magnetopause and P_d, B_z, B, and N during the entire evolution of the moderate storm on August 4, 2010.

3.5.1. *Case of the minor CME storm: April 20, 2014*

A detailed analysis of the minor ICME storm of 20 April 2014 is conducted as a reference case. Figure 6 shows the linear and non-linear correlations and regressions between the magnetopause subsolar position (R_o) and solar wind parameters throughout the event. Table 3 summarises the statistical robustness and fidelity indicators for the associated models.

The results confirm the models of Refs. [4, 23]: dynamic pressure (P_d) is the main driver of the dynamics of the Earth's subsolar magnetopause position (R_o) during this event. The

Table 6. Indicators of statistical robustness and model fidelity (linear and polynomial) of the influence of solar wind parameters on R_o during the complete evolution of the moderate ICME storm of 4 August 2010.

Parameters	Neff	r	IC95%	p-value	RMSE Lin ($\pm\sigma$)	RMSE Poly2 ($\pm\sigma$)
(P_d, R_o)	84.2	-0.85	[-0.90, -0.77]	0	1.63 ± 2.12	10.62 ± 20.38
(B_z, R_o)	94.2	0.23	[0.03, 0.41]	0.0263	1.38 ± 0.77	0.98 ± 0.49
(B, R_o)	68.2	-0.78	[-0.86, -0.66]	7.55×10^{-15}	1.04 ± 0.73	2.33 ± 3.13
(N, R_o)	85.5	-0.85	[-0.90, -0.78]	0	0.73 ± 0.46	1.46 ± 2.20

Table 7. Correlation and regression coefficient values between R_o and solar wind parameters during moderate ICMEs ICME 2 (2 October 2013) and 3 (6 November 2015).

Events	Moderate storm 2			Moderate storm 3		
Indicators of dependency	Corr(r)	Linear (R^2)	Poly^2 (R^2)	Corr(r)	Linear (R^2)	Poly^2 (R^2)
(R_o, P_d)	-0.66	0.44	0.68	-0.86	0.75	0.85
(R_o, N)	-0.76	0.58	0.73	-0.80	0.63	0.69
(R_o, B)	-0.52	0.27	0.27	-0.14	0.02	0.02
(R_o, B_z)	0.37	0.14	0.17	0.44	0.20	0.45

Table 8. Indicators of statistical robustness and model fidelity (linear and polynomial) of the influence of solar wind parameters on R_o during the complete evolution of moderate ICME storms 2 (02-10-2013) and 3 (06-11-2015).

Events	Parameters	Neff	r	IC95%	p-value	RMSE Lin ($\pm\sigma$)	RMSE Poly2 ($\pm\sigma$)
Moderate storm 2	(P_d, R_o)	53.7	-0.66	[-0.79, -0.48]	5.63×10^{-8}	2.91 ± 2.07	13.91 ± 24.77
	(B_z, R_o)	83.6	0.37	[0.17, 0.54]	5.40×10^{-4}	2.42 ± 1.10	2.31 ± 1.17
	(B, R_o)	48.5	-0.52	[-0.70, -0.27]	1.56×10^{-4}	2.07 ± 1.33	4.74 ± 4.59
	(N, R_o)	51.8	-0.76	[-0.86, -0.62]	5.92×10^{-11}	1.76 ± 1.01	1.57 ± 1.10
Moderate storm 3	(P_d, R_o)	76.5	-0.86	[-0.91, -0.79]	0	0.53 ± 0.26	0.44 ± 0.20
	(B_z, R_o)	93.6	0.44	[0.26, 0.59]	8.26×10^{-6}	0.90 ± 0.45	1.02 ± 0.67
	(B, R_o)	67.1	-0.14	[-0.37, 0.11]	0.266	1.20 ± 0.65	2.17 ± 1.76
	(N, R_o)	81.6	-0.80	[-0.86, -0.70]	0	0.61 ± 0.30	0.69 ± 0.37

Table 9. Indicators of statistical robustness and model fidelity (linear and polynomial) of the influence of solar wind parameters on R_o during the entire evolution of the strong ICME storm of 23 June 2015.

Parameters	Neff	r	IC95%	p-value	RMSE Lin ($\pm\sigma$)	RMSE Poly2 ($\pm\sigma$)
(P_d, R_o)	59.5	-0.73	[-0.83, -0.59]	3.62×10^{-11}	2.51 ± 1.42	8.67 ± 9.27
(B_z, R_o)	92.9	0.13	[-0.08, 0.32]	0.231	2.00 ± 0.32	3.49 ± 2.29
(B, R_o)	58.5	-0.64	[-0.77, -0.46]	5.81×10^{-8}	1.78 ± 0.78	2.96 ± 2.18
(N, R_o)	58.1	-0.73	[-0.83, -0.58]	7.10×10^{-11}	1.40 ± 0.32	3.76 ± 4.50

Table 10. Correlation and regression coefficient values between R_o and solar wind parameters during the strong ICME storm 2 (24-10-2011) and 3 (14-07-2012).

Parameters	Strong storm 2			Strong storm 3		
Dependency indicators	Corr(r)	Linear (R^2)	Poly^2 (R^2)	Corr(r)	Linear (R^2)	Poly^2 (R^2)
(R_o, P_d)	-0.92	0.84	0.95	-0.68	0.46	0.63
(R_o, N)	-0.86	0.74	0.75	-0.68	0.46	0.56
(R_o, B)	-0.47	0.22	0.25	-0.68	0.47	0.48
(R_o, B_z)	0.34	0.12	0.39	0.52	0.27	0.39

strong anticorrelation (r = −0.91), validated by a Neff = 77.3 (p = 0), demonstrates a robust physical link after autocorrelation correction. The second-order polynomial fit (RMSE = 0.35±0.16) outperforms the linear model (0.59±0.26), reflecting the non-linear nature of plasma compression during this minor ICME.

Conversely, the absence of correlation with B_z (r = −0.01; p = 0.946) attests to an exclusively mechanical process regime. In accordance with Ref. [34], the oscillation of B_z around zero prevents any coupling by effective magnetic reconnection. Although the influence of total intensity B remains secondary (r = −0.58), its linear response (RMSE = 1.28±0.23) validates a transfer of momentum without curvature effects, in agreement with the simulations of Ref. [20]. At the same time, the density N shows a critical polynomial dependence (r = −0.89; RMSE = 0.49±0.20), isolating the compressed structures at the shock front.

The robustness of our results is underscored by their con-

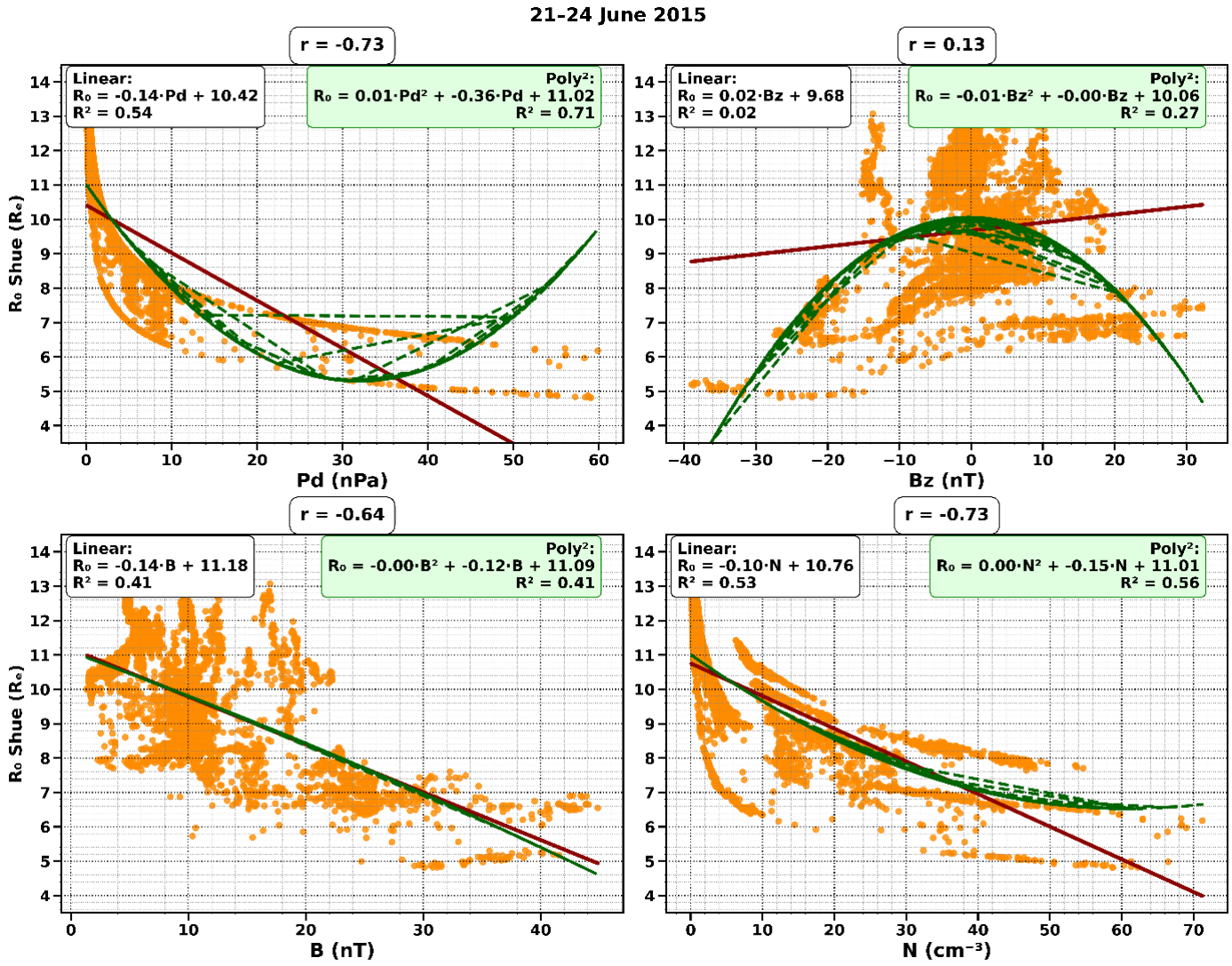

Figure 8. Correlation and linear and nonlinear regression between the subsolar location R_o of the Earth's magnetopause and P_d, B_z, B, and N during the entire evolution of the strong storm on June 23, 2015.

Table 11. Indicators of statistical robustness and model fidelity (linear and polynomial) of the influence of solar wind parameters on R_o during the complete evolution of strong ICME storms 2 (24-10-2011) and 3 (14-07-2012).

Events	Parameters	Neff	r	IC95%	p-value	RMSE Lin ($\pm\sigma$)	RMSE Poly2 ($\pm\sigma$)
Strong storm 2	(P_d, R_o)	48.2	-0.92	[-0.95, -0.86]	0	0.78 ± 0.51	1.11 ± 1.55
	(B_z, R_o)	54	0.34	[0.08, 0.56]	0.0109	1.37 ± 0.53	1.27 ± 0.52
	(B, R_o)	44.8	-0.47	[-0.67, -0.20]	1.31×10^{-3}	1.32 ± 0.51	1.83 ± 1.33
	(N, R_o)	48.6	-0.86	[-0.92, -0.77]	2.89×10^{-15}	0.71 ± 0.39	0.79 ± 0.38
Strong storm 3	(P_d, R_o)	80	-0.68	[-0.78, -0.54]	5.46×10^{-12}	4.45 ± 5.24	69.54 ± 136.01
	(B_z, R_o)	80.1	0.52	[0.33, 0.66]	9.80×10^{-7}	2.15 ± 0.58	2.65 ± 1.51
	(B, R_o)	74.9	-0.68	[-0.79, -0.54]	1.51×10^{-11}	2.78 ± 1.62	3.07 ± 2.04
	(N, R_o)	81.2	-0.68	[-0.78, -0.54]	2.44×10^{-12}	2.40 ± 1.32	14.29 ± 25.27

sistency with the statistical study by Ref. [8]. Despite different methodologies and models, Ref. [35] versus Ref. [5], our event coefficients (r = −0.91 for P_d, r = −0.89 for N, and r = −0.58 for B corroborate the long-term annual averages. Our approach, with its high-resolution and temporal-persistence correction, rigorously demonstrates that the insensitivity of R_o to B_z is not an artefact but a sign of 'cold' (purely mechanical) compression dominating reconnection during this minor ICME storm in cycle 24.

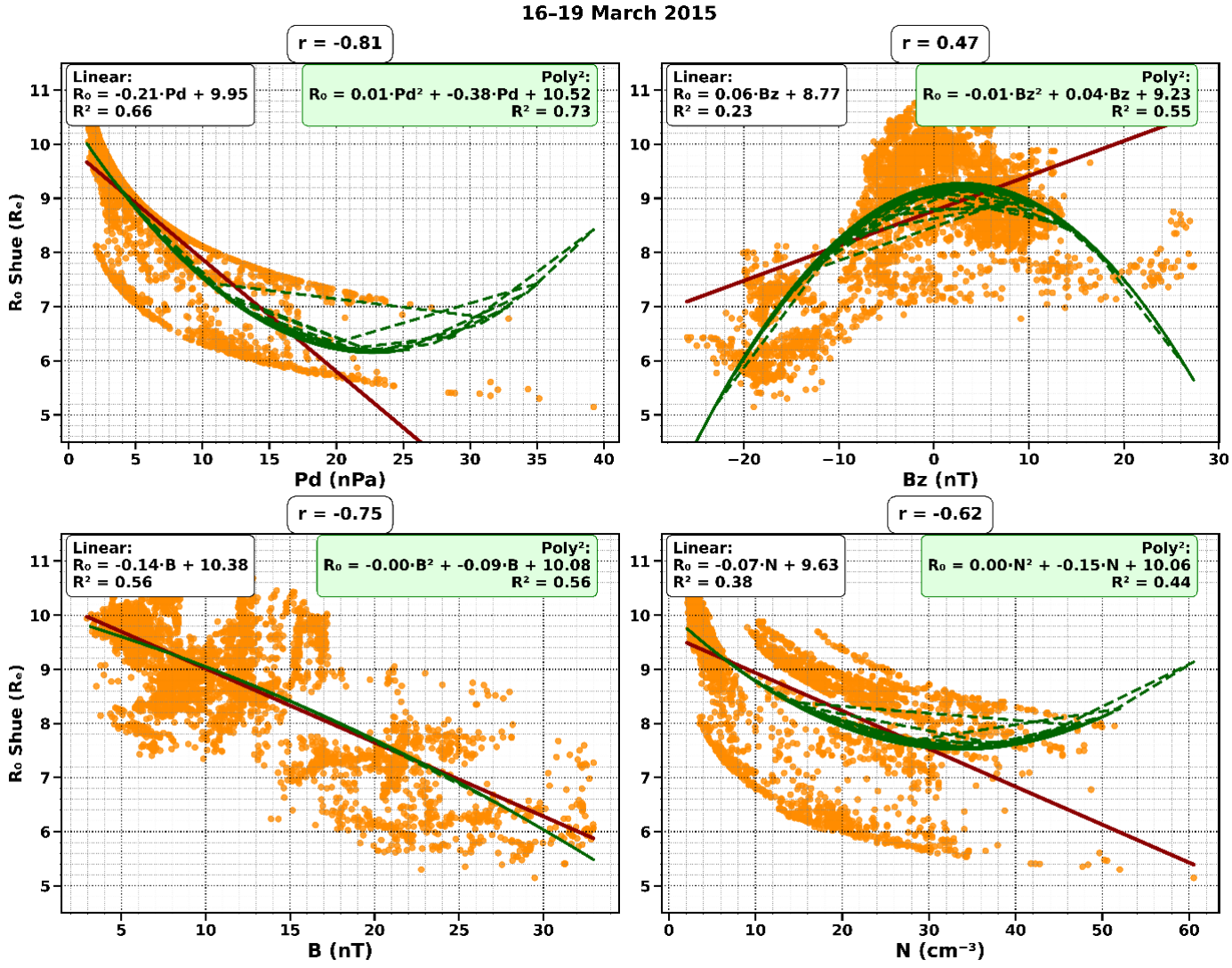

Figure 9. Correlation and linear and nonlinear regression between the subsolar location R_o of the Earth's magnetopause and P_d, B_z, B, and N during the entire evolution of the extreme storm of March 17, 2015.

Table 12. Indicators of statistical robustness and model fidelity (linear and polynomial) of the influence of solar wind parameters on R_o during the entire evolution of the extreme ICME storm of 17 March 2015.

Parameters	Neff	r	IC95%	p-value	RMSE Lin ($\pm\sigma$)	RMSE Poly2 ($\pm\sigma$)
(P_d, R_o)	52.6	-0.81	[-0.89, -0.70]	1.71×10^{-13}	0.72 ± 0.35	0.72 ± 0.48
(B_z, R_o)	58.1	0.47	[0.25, 0.65]	1.65×10^{-4}	1.27 ± 0.42	0.94 ± 0.31
(B, R_o)	46.7	-0.75	[-0.85, -0.58]	2.16×10^{-9}	1.16 ± 0.78	0.94 ± 0.33
(N, R_o)	50.5	-0.62	[-0.76, -0.41]	1.51×10^{-6}	1.01 ± 0.57	0.99 ± 0.63

Comparative analysis: minor CME storms. Following a detailed analysis of the moderate ICME storm of 20 April 2014, considered here as event number 1 in the category (ICME 1), the study is extended to two other events of the same intensity, ICME 2 (2 October 2013) and ICME 3 (6 November 2015), in order to assess the consistency of the mechanisms identified. Tables 4 and 5 summarise the results associated with these two events.

The correlations with kinetic parameters (P_d and N) are robust (r ≈ −0.85 to −0.91), as evidenced by significant Neff values and p-values of 0, ruling out any autocorrelation artefacts.

The analysis of root mean square errors (RMSE) provides a critical nuance to the modelling: while the non-linear response to dynamic pressure is confirmed, the numerical instability of the polynomial model for event 2 (RMSE = 14.08±27.22) reveals a risk of overfitting. In this context, linear adjustment proves more robust for describing the Ref. [21] equilibrium, in which the boundary continuously adjusts to the incident plasma load.

Regarding the total interplanetary magnetic field (B), its

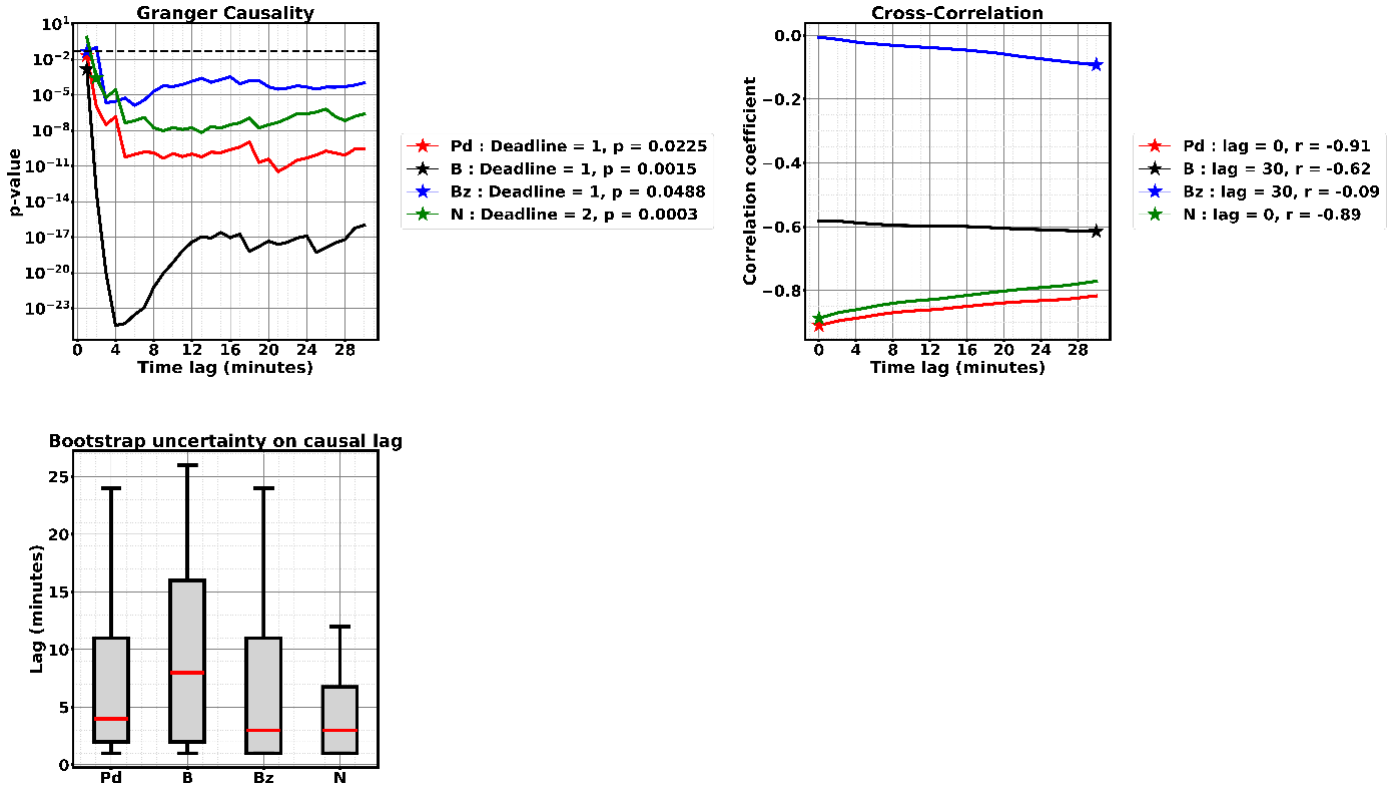

Figure 10. Cross-correlation and Granger causality of R_o dynamics under the influence of P_d, B, B_z, and N during the minor ICME storm of 20 April 2014. The dotted black horizontal line (upper left graph) indicates the significance threshold ($p < 0.05$).

role in compressing the magnetopause is reflected in a systematic but heterogeneous anticorrelation (r = −0.58, −0.35, and −0.76). This variability, confirmed by p-values <0.01, suggests that the effectiveness of B depends on the internal structure of the ICME (particularly the sheath). Unlike the annual averages reported in [8], our event-based approach shows that B acts as a simple additive component in the pressure balance, without additional structural complexity, and that the linear model remains the most effective here.

Finally, the influence of the B_z component is statistically zero in all three cases. The coefficients r ≈ 0, the p-values well above (>0.05) and the confidence intervals surrounding zero (0) demonstrate the inactivity of magnetic reconnection. The magnetopause then acts as an impermeable interface, insensitive to the orientation of the interplanetary magnetic field. These results corroborate the conclusions of Ref. [36]: for minor storms, dynamic pressure largely prevails over directional electromagnetic forces in controlling the dynamics of the magnetopause's subsolar position (R_o).

Case of the moderate CME storm: August 4, 2010. A detailed analysis of the moderate ICME storm of 4 August 2010 is conducted as a reference case. Figure 7 shows the linear and non-linear correlations and regressions between R_o and solar wind parameters throughout the event. Table 6 summarises the statistical robustness and fidelity indicators for the associated models.

Analysis of this moderate ICME storm reveals a transitional regime: the dynamics of the subsolar magnetopause (R_o) depart from simple pressure equilibrium and incorporate global MHD processes. While the dynamic pressure (P_d) and density (N) of the solar wind remain a driving force (r = −0.85; p-values = 0), the RMSE analysis rejects the polynomial fit for P_d. Despite a high R^2 (0˙87˙), the substantial increase in RMSE (10.62±20.38) indicates severe overfitting. The superiority of the linear model (1.63±2.12) demonstrates that the magnetopause responds proportionally to the forcing, indicating the absence of complex non-linear processes or abrupt phase transitions.

The influence of the interplanetary magnetic field intensity (B) is significant here, confirming the amplifying role of solar wind magnetic pressure described by Ref. [20]. This contribution follows a linear superposition law, reinforcing mechanical compression without distorting the cavity's structure. Unlike the three (03) minor cases studied, the B_z component shows a statistically significant influence (r = 0.23; p-value = 0.0263). The improvement in RMSE by the polynomial model (0.98 versus 1.38) suggests the onset of a non-linear response linked to incipient magnetic reconnection. However, the event remains 'non-erosive'; in accordance with Ref. [34], the absence of a prolonged southward orientation of B_z prevents large-scale reconnection from dominating the dynamics of the boundary.

The convergence of our results with the annual averages of [8] (r = −0.78 versus −0.588 for B) indicates that the magnetic field effect is intensified by the moderate nature of the shock

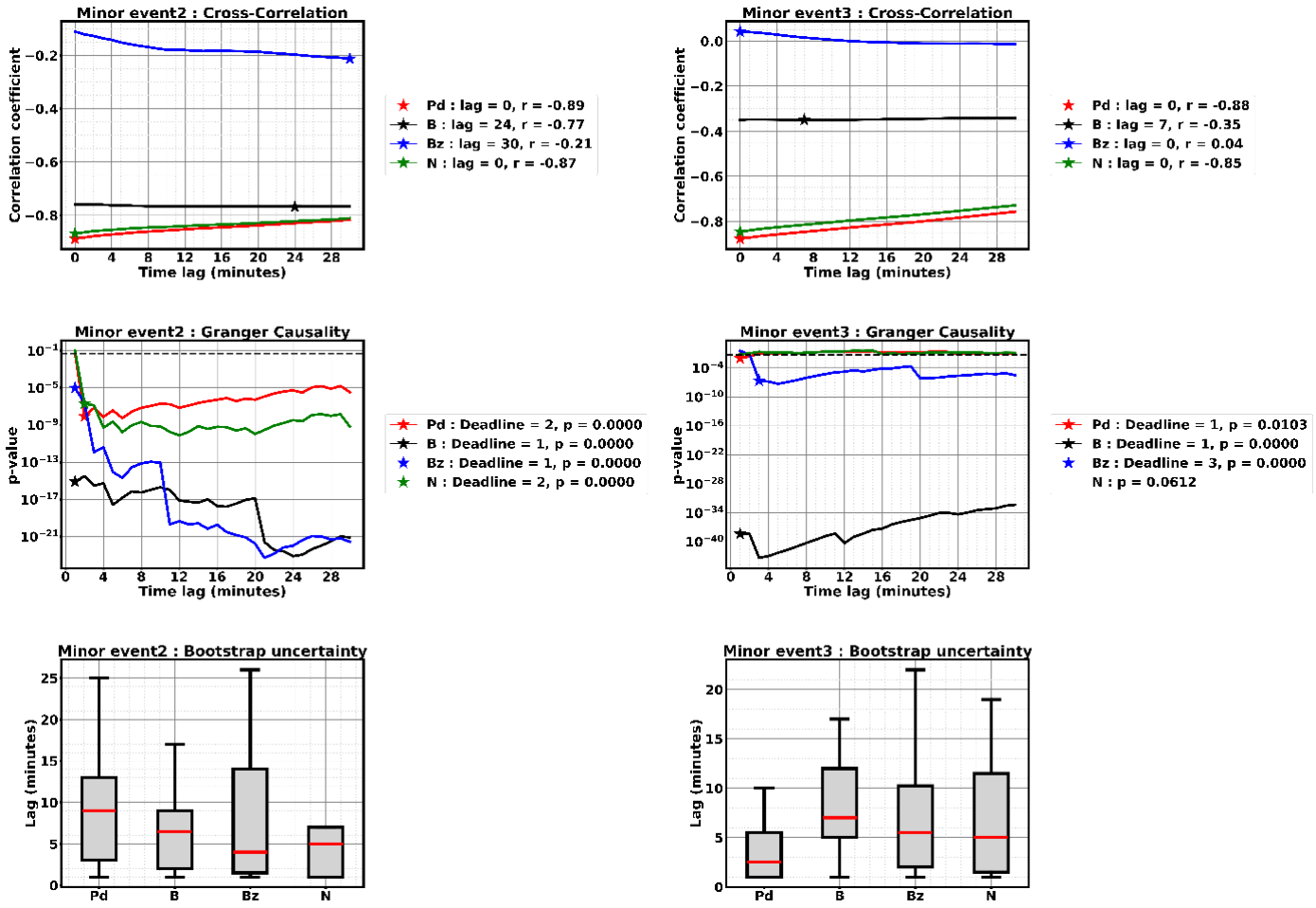

Figure 11. Cross-correlation and Granger causality of *Ro* dynamics under the influence of *Pd*, B, B_z, and N for minor ICME storms 2 (5 June 2011) and 3 (9 March 2018). The dotted black horizontal line (causality graphs) indicates the significance threshold ($p < 0.05$).

structure. Thus, although B_z becomes a conditional factor, the compression of the magnetopause during this moderate ICME storm remains governed by mechanical factors, with the linear model providing the most robust physical description of the processes at work.

Comparative analysis: moderate CME storms. Following a detailed analysis of the moderate ICME storm of 4 August 2010, considered here as event number 1 in the category (ICME 1), the study is extended to two other events of the same intensity, ICME 2 (2 October 2013) and ICME 3 (6 November 2015), in order to assess the consistency of the mechanisms identified. Tables 7 and 8 summarise the results associated with these two events.

The comparative study of the three moderate ICME events in solar cycle 24 confirms that the dynamics are still dominated by kinetic parameters (P_d, N), but marks a transition towards complex coupling. The robust anti-correlations ($r \approx -0.66$ to -0.86; p-values ≈ 0) validate the persistence of mechanical control. However, RMSE analysis reveals critical instability in second-order polynomial models (e.g., RMSE = 13.91±24.77 for event 2 as for event 1), highlighting a risk of overfitting. In this moderate regime, linear modelling is the most robust method for describing the response of R_o to dynamic pressure (P_d), avoiding numerical artefacts.

The influence of the interplanetary magnetic field intensity (B) is irregular ($r = -0.78$ to -0.14) and strictly dependent on the internal structure of the compression sheath. The absence of a significant correlation for event 3 ($p = 0.266$) confirms that B is not a universal predictor, but a secondary contextual factor in these three cases of moderate ICME storm events in solar cycle 24.

The salient feature in this section is the emergence of a significant dependence on B_z ($r = 0.23$ to 0.44). Unlike the minor cases studied, the greater stability of the polynomial models here suggests a gradual activation of magnetic reconnection at the day-side magnetopause. This transition indicates that during these three moderate geomagnetic storms of CME origin, the magnetopause ceases to be a simple pressure barrier and becomes a dynamic interface where reconnection (B_z<0) and compression (P_d) processes intertwine, altering the overall morphology of the magnetospheric cavity.

Case of the intense CME storm: June 23, 2015. A detailed analysis of the strong ICME storm of 22 June 2015 is conducted as a reference case. Figure 8 shows the linear and non-linear

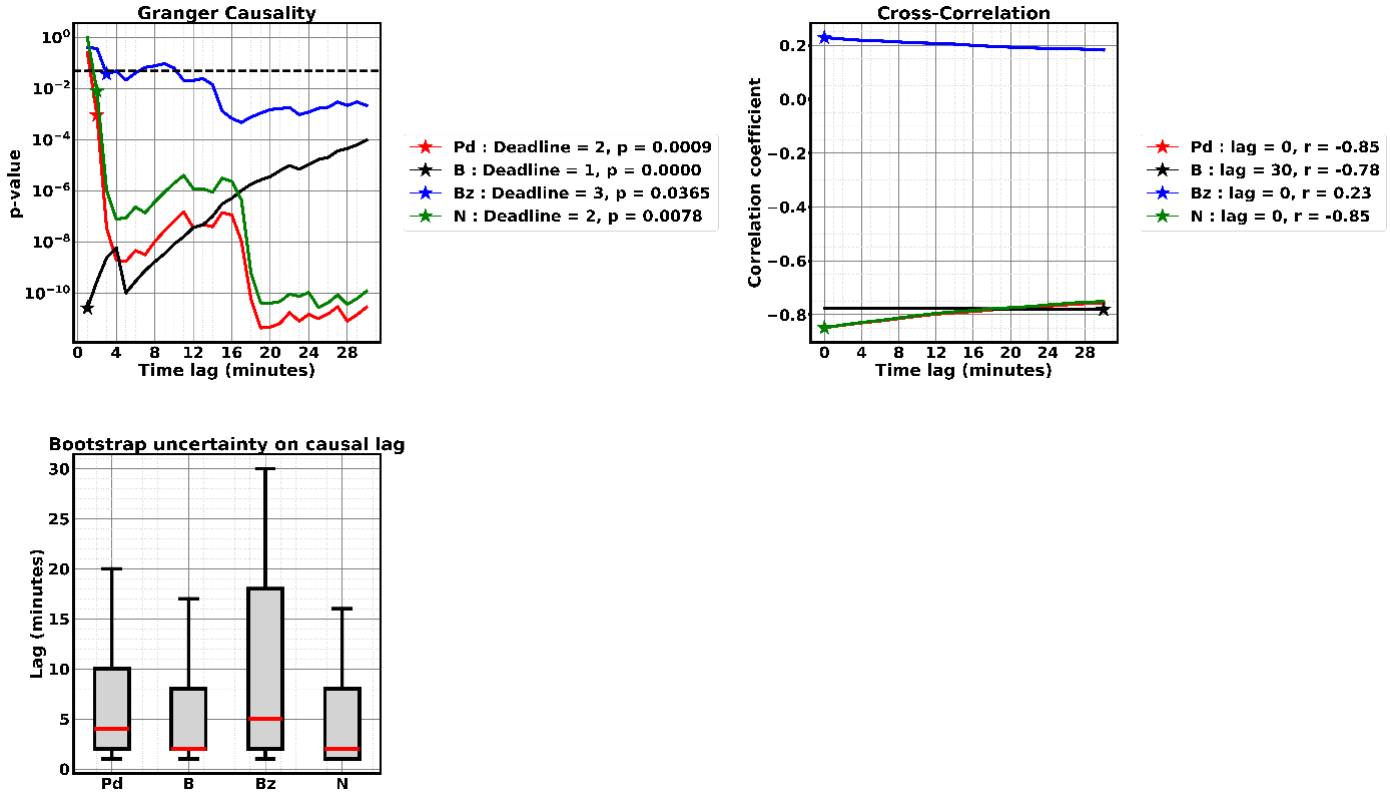

Figure 12. Cross-correlation and Granger causality of *Ro* dynamics under the influence of *Pd*, B, B_z, and N during the moderate ICME storm of 4 August 2010. The dotted black horizontal line (upper left graph) marks the significance threshold ($p < 0.05$).

correlations and regressions between R_o and solar wind parameters throughout the event. Table 9 summarises the indicators of statistical robustness and modelling fidelity in linear and non-linear terms.

The study of this strong ICME storm reveals a counterintuitive dynamic in which, despite the event's intensity, control of the dynamics of the subsolar position (R_o) of the Earth's magnetopause remains dictated by mechanical rather than erosive effects. Dynamic pressure (P_d) and density (N) show a robust negative correlation (r = −0.73; p-value = 10^{-11}). However, the RMSE explosion for the polynomial model (8.67±9.27 versus 2.51±1.42 for the linear model) indicates severe overfitting. This result shows that during this violent shock, R_o follows a quasi-linear power law, rendering the second-degree fit physically irrelevant.

The influence of the total interplanetary magnetic field (B) is notable (r = −0.64), acting as an amplifier of mechanical effects in accordance with the simulations of Ref. [20]. The superiority of the linear model (RMSE = 1.78 versus 2.96 for the polynomial) suggests that the magnetic pressure adds coherently to P_d at the shock front, maximising the compression of the magnetopause.

Conversely, component B_z shows a marginal correlation (r = 0.13; p-value = 0.231). This result, coupled with the instability of the polynomial model, confirms the absence of magnetopause erosion. This shows that the dynamics of R_o in this case of extreme ICME storm are governed by mechanical compression effects and can be explained by the internal structure of the responsible ICME: a rapid northward shift of B_z after a strong southward incursion ($B_z < 0$) prevented any sustained electromagnetic coupling. This finding qualifies the work of Ref. [34] by demonstrating that erosion is conditioned by the duration of the southward orientation of, and not solely by the intensity of the shock. These results highlight the need to distinguish between 'impulsive-compressive' events and 'energetic-erosive' events, as the brute force of an ICME does not systematically guarantee proportional erosion.

Comparative analysis: cases of strong CMEs. Following a detailed analysis of the strong ICME storm of 22 June 2015, referred to here as event (ICME 1), the study was extended to two other events of the same intensity, ICME 2 (24 October 2011) and ICME 3 (14 July 2012), in order to assess the consistency of the mechanisms identified. Tables 10 and 11 summarise the results associated with these two events.

The comparative study of the three major ICME storms during cycle 24 demonstrates that the subsolar position (R_o) of the Earth's magnetopause remains determined by mechanical compression, despite the intensity of the magnetic fields in the solar wind. Dynamic pressure (P_d) and density (N) maintain extremely robust anti-correlations (r up to −0.92; p-values = 0). A major modelling observation is required: the collapse of polynomial models for event 3 (RMSE = 69.54 versus 4.45 in the linear model) confirms that the magnetopause responds impulsively and linearly to P_d. Attempting to adjust for non-linear

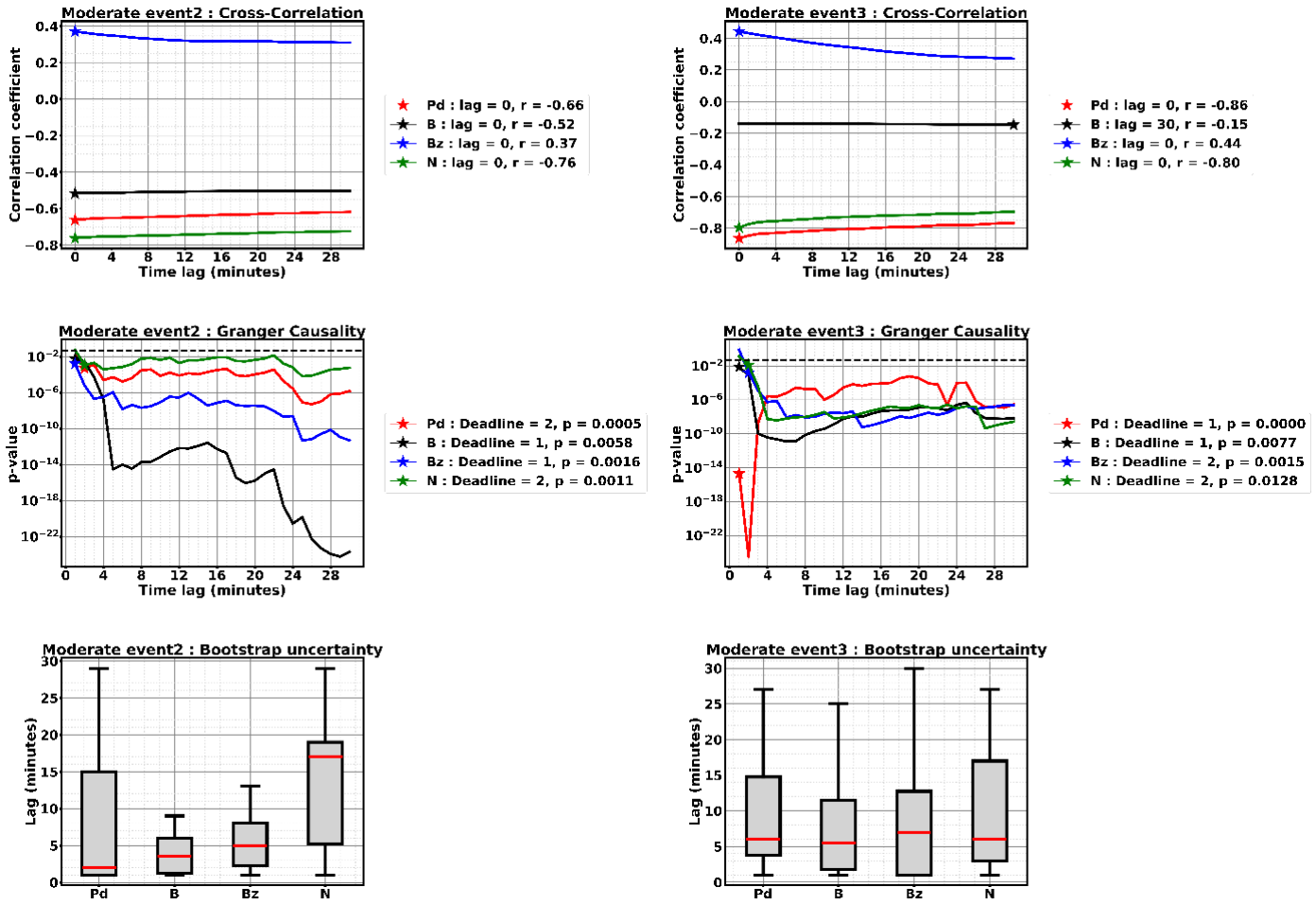

Figure 13. Cross-correlation and Granger causality of *Ro* dynamics under the influence of *Pd*, B, B_z, and N during moderate ICME storms 2 (October 2, 2013) and 3 (November 6, 2015). The dotted black horizontal line (causality graphs) indicates the significance threshold ($p < 0.05$).

curvature leads to overfitting with no physical basis, as linearity remains the most accurate descriptor of the boundary's resilience under these conditions.

In accordance with the simulations by Ref. [20], the intensity of the total interplanetary magnetic field (B) exerts a stabilising influence (r from −0.47 to −0.68). Unlike the minor and moderate cases studied, B acts here as a constant additive pressure within the compression sheath, reinforcing the magnetopause's compression. The stability of the linear RMSEs (1.32 to 2.78) validates this magnetic contribution.

Finally, although dependence on B_z appears to be increasing (r up to 0.52; $p<0.05$), actual magnetic erosion remains marginal compared to the mechanical effects of magnetopause compression. The analysis reveals a crucial aspect of the internal structure of these ICMEs responsible for the storms studied: the effectiveness of erosion does not depend solely on the intensity of the southern B_z, but on its temporal stability in its southern orientation. A rapid shift to the north is sufficient to cancel out the erosive impact, leaving plasma pressure as the sole driver of magnetopause displacement. These results require a rigorous distinction in space weather between mechanical compression and magnetopause erosion by reconnection.

Case study: Extreme CME storm: March 17, 2015. The detailed analysis of the extreme ICME storm of 17 March 2015, known as the 'Saint Patrick's Day Storm', is conducted as a single case representative of the extreme category of solar cycle 24. Figure 9 shows the linear and non-linear correlations and regressions between solar wind parameters throughout the event. Table 12 summarises the statistical robustness and fidelity indicators for the associated models.

Analysis of the extreme ICME storm of 17 March 2015 reveals an unprecedented synergy in which electromagnetic coupling reaches a saturation threshold, rivalling the mechanical compression effects of the Earth's magnetopause. Unlike the minor strong regimes studied, this extreme case requires polynomial adjustment as the optimal descriptor. For dynamic pressure (P_d), although the RMSEs are close, the polynomial model significantly improves the explained variance ($R^2 = 0.73$), capturing the physical non-linearity specific to this extreme shock.

The influence of total intensity B (r = −0.75) and density N (R^2 polynomial of order 2 = 0.55) confirms the influence of B. In agreement with Ref. [20], B acts as an additive pressure to the dynamic pressure and, in this extreme case, also improves the efficiency of magnetic reconnection. The major find-

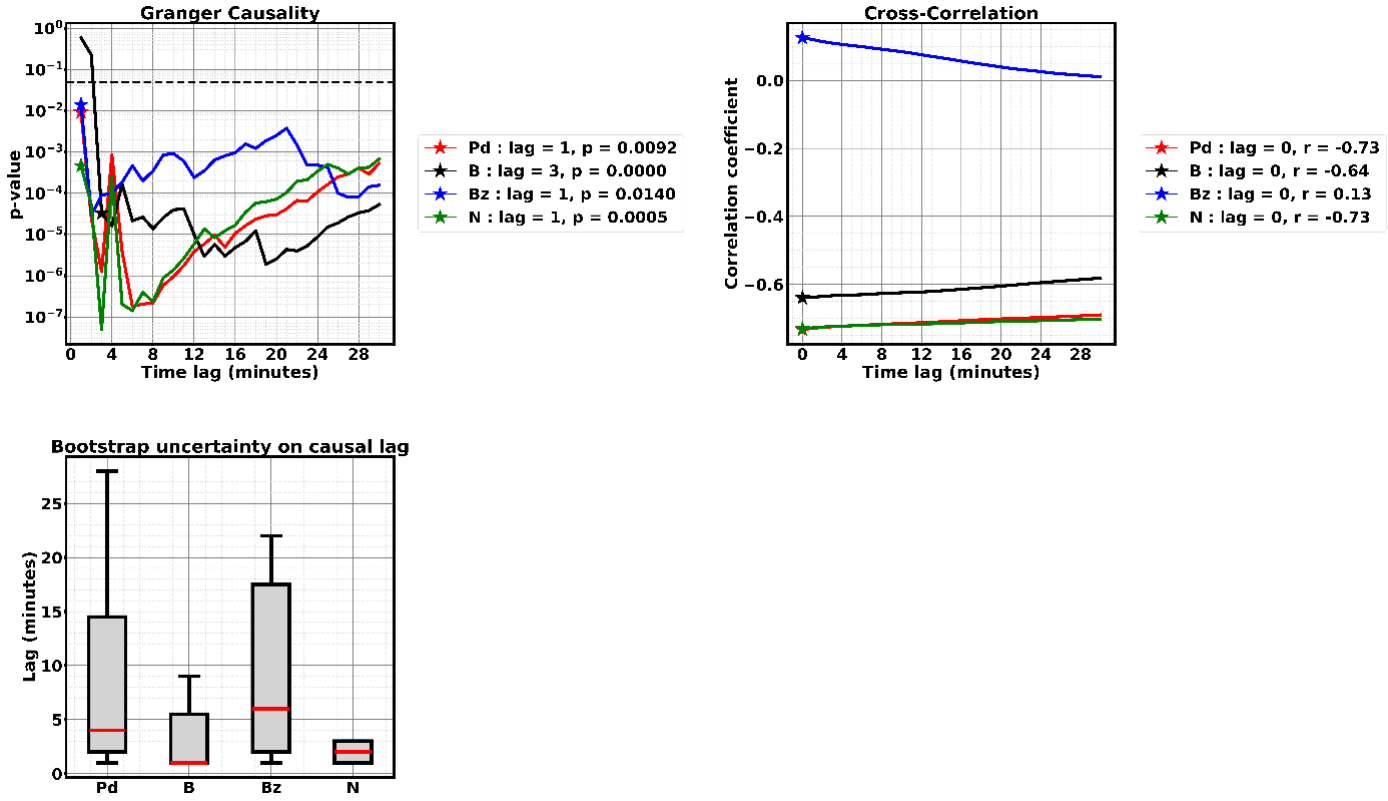

Figure 14. Cross-correlation and Granger causality of *Ro* dynamics under the influence of *Pd*, B, B_z, and N during the strong ICME storm of 22 June 2015. The dotted black horizontal line (upper left graph) indicates the significance threshold ($p < 0.05$).

ing in this extreme CME storm case remains the behaviour of B_z: its highly significant positive correlation (r = 0.47; p-value = $1.65.10^{-4}$) and the explosion of its coefficient of determination (0.23 to 0.55 in polynomial) indicate highly active reconnection. In line with the work of Refs. [25, 34], the prolonged southward orientation of B_z induced magnetopause erosion via the activation of Birkeland currents, pushing the magnetopause below the geosynchronous orbit.

This study, covering ten events in solar cycle 24, demonstrates that while the response to P_d is predominantly linear in the minor-to-strong cases studied, it converges towards non-linearity in the extreme case. This finding validates the historical evolution of the model developed by Ref. [5]: linearity fails to reproduce the extreme compressions observed by Geotail and Interball-1. Our results establish the superiority of polynomial formulations for capturing saturation effects and require abandoning linear extrapolations in favour of saturated dynamic models, which are essential for reliable operational space weather forecasting in typical cases of this extreme ICME storm.

3.6. *Cross-correlation analysis, time delay, and Granger causality between the subsolar position $\boldsymbol{R_o}$ of the Earth's magnetopause and solar wind parameters*

To better characterise the magnetopause response during the ICME events studied, we analyse cross-correlations and Granger causality between the solar wind parameters (P_d, B, B_z, and N). This approach, reinforced by uncertainty estimation via bootstrap, allows us to distinguish the predictive coupling delay from the maximum response time for each parameter. By isolating these time scales, we provide a more detailed interpretation of the dynamics of R_o under ICME constraints.

Case of the minor storm of April 20, 2014. The combined analysis of cross-correlation, Granger causality testing, and bootstrap uncertainties enables characterisation of the temporal response dynamics of (R_o) to fluctuations in solar wind parameters during the minor ICME storm of 4 August 2010 (Figure 10).

Granger causality and cross-correlation analysis in this minor ICME storm reveal that variations in (P_d, N) precede those in R_o by 1 to 2 minutes and significantly influence these variations in R_o. The analysis also shows that R_o responds to these mechanical compression constraints, and that their effects are optimised immediately ($r \approx -0.91$ at a lag of 0 min). This confirms and validates that plasma mechanical forces are the most stable predictors of R_o dynamics during this minor ICME storm, a robustness validated by the tight Bootstrap distributions.

The results also show a phase corresponding to structural consolidation driven by the interplanetary magnetic field (IMF). Although the variations in B and B_z precede those in R_o (1 min) in this case of a minor ICME storm, the influence of B is significant, and that of B_z is marginal. As for the effects of B (solar wind magnetic pressure) on R_o, they only optimise after a 30-

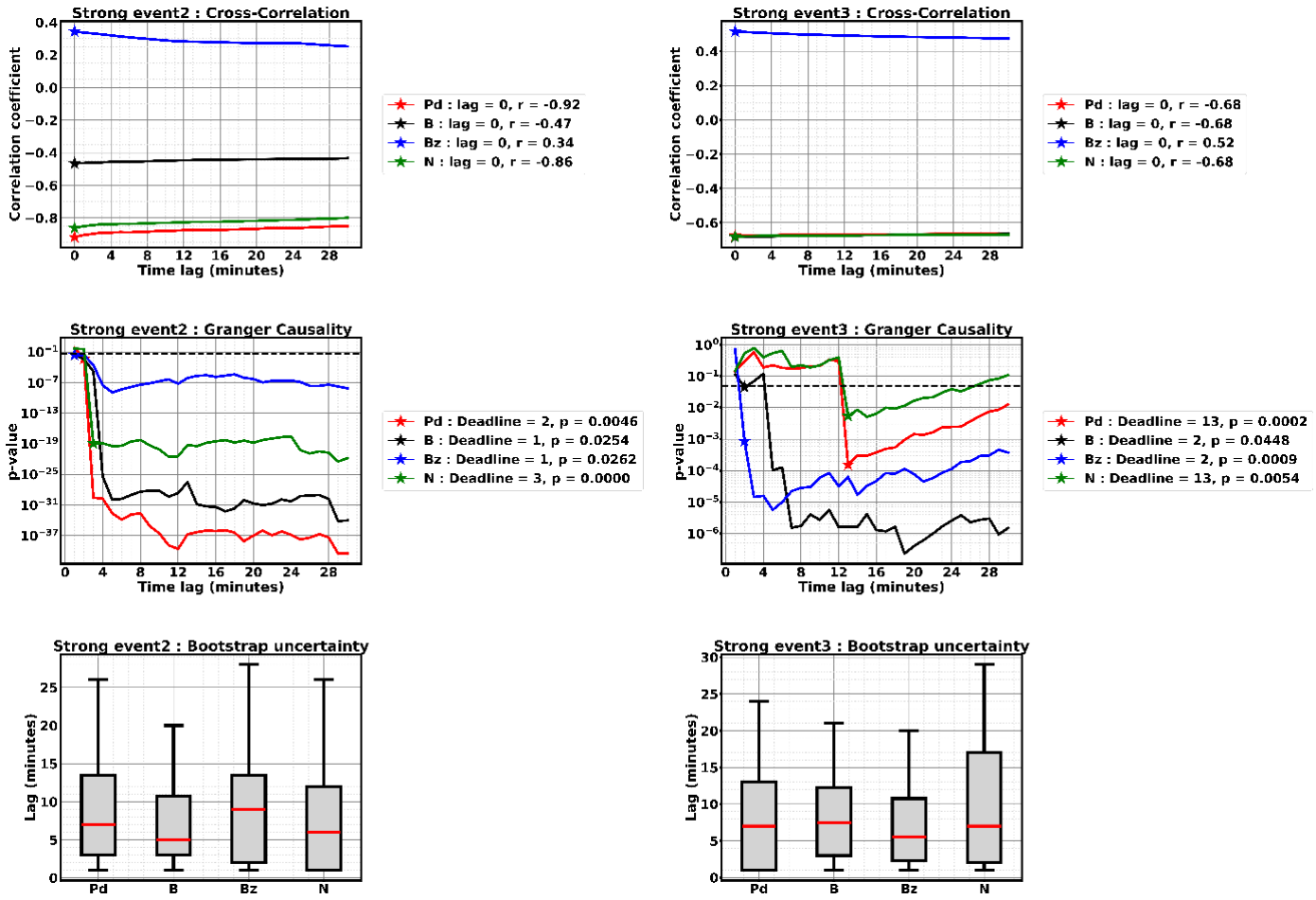

Figure 15. Cross-correlation and Granger causality of *Ro* dynamics under the influence of *Pd*, B, B_z, and N during strong ICME storms 2 (24 October 2011) and 3 (14 July 2012). The dotted black horizontal line (causality graphs) indicates the significance threshold ($p < 0.05$).

minute maturation period ($r = -0.62$). This delay reflects the time required for global magnetohydrodynamic adjustments, including flux convection and magnetosheath stabilisation.

Thus, the dynamics of R_o in this case of a minor ICME event studied can be summarised as instantaneous mechanical compression, reinforced by a delayed structural adjustment dictated by the magnetic configuration of the responsible ICME.

Comparative cross-correlation analysis: case of minor CME storms. After analysing Case 1, a comparative study was conducted with Cases 2 and 3 (Figure 11). This combined approach allows distinguishing the predictive coupling delay (Granger) from the maximum response time of R_o to each solar wind parameter.

Comparative analysis of the three minor ICME storms in solar cycle 24 reveals a stable dynamic hierarchy dominated by mechanical compression. In all cases, dynamic pressure (P_d) emerges as the universal driver, with maximum anticorrelation at lag = 0 min and quasi-instantaneous Granger causality (1 min to 2 min). This behaviour validates the immediate mechanical compression predicted by Ref. [21]. While density (N) generally follows this temporal linearity, the anomaly in case 3 (loss of causal significance, $p \approx 0.06$) suggests a saturation regime in which the information carried by N becomes redundant for predicting R_o.

For IMF B intensity, its variations precede R_o variations by 1 min and significantly influence them. The maximum response of R_o to this constraint manifests itself with a delay that varies according to the internal structures of the three minor ICME events: a 30-minute delay (cases 1 and 2), which can be explained by an accumulation of magnetic flux in the magnetosphere slowing down the transmission of the magnetic signal, while the 7-minute delay associated with the low correlation ($r = -0.35$) in case 3 can be explained by a rapid but inefficient transfer, probably linked to early reconnection in the magnetosheath, dissipating part of the incident energy before it reaches the magnetopause [37].

Finally, although variations in B_z precede those in R_o, its influence remains marginal and delayed in the three cases of minor ICME storms. The 30-minute delay (cases 1 and 2) confirms this and suggests that B_z does not act directly and immediately on the subsolar position, but rather through slower internal processes. As Refs. [7, 38] point out, this delay reflects the time required for tail currents to activate and for the magnetospheric hysteresis effect to occur, thereby delaying the response of R_o.

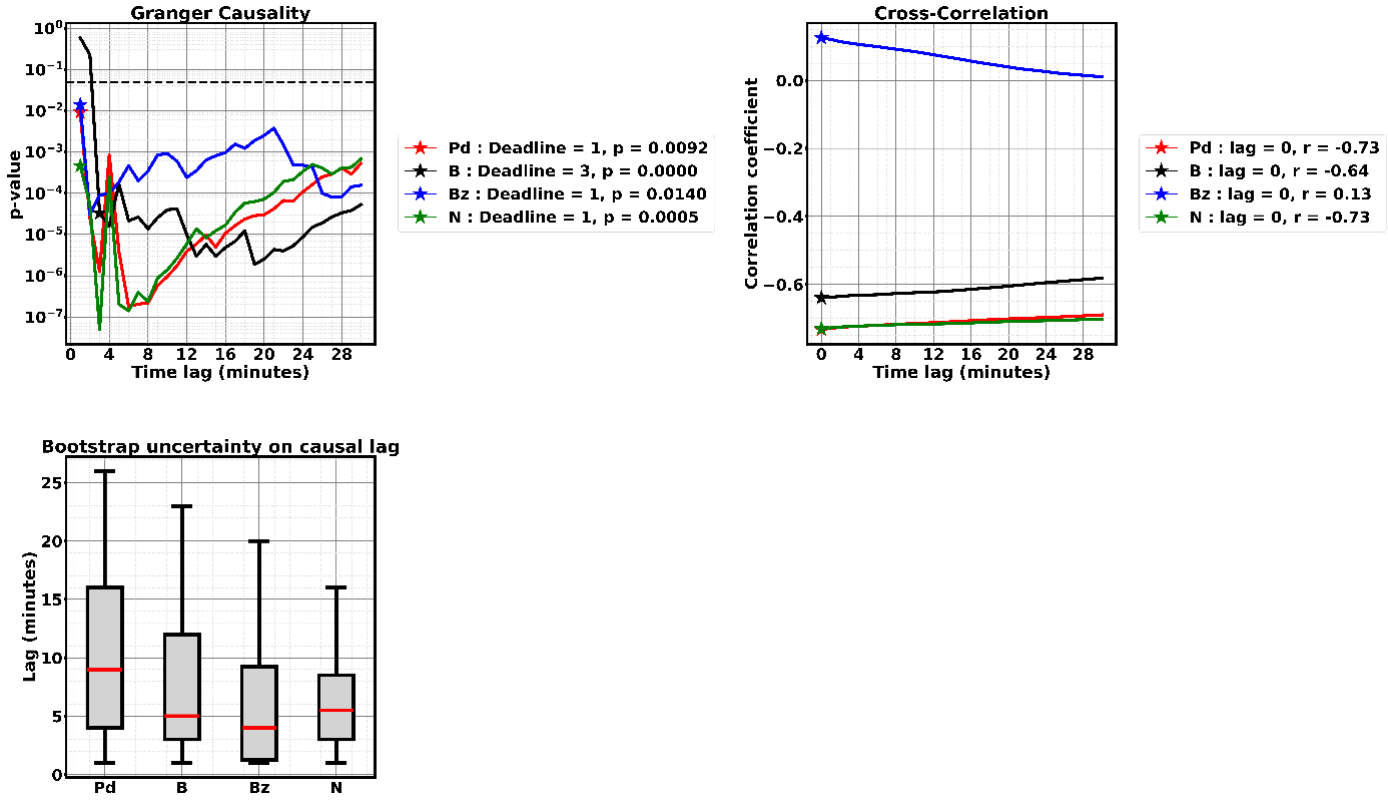

Figure 16. Cross-correlation and Granger causality of *Ro* dynamics under the influence of *Pd*, B, B_z, and N during the extreme storm of 17 March 2015. The dotted black horizontal line (upper left graph) indicates the significance threshold ($p < 0.05$).

Case of the moderate storm of 4 August 2010. The combined analysis of cross-correlation, Granger causality testing and bootstrap uncertainties makes it possible to characterise the temporal response dynamics of (R_o) to variations in solar wind parameters during the moderate ICME storm of 4 August 2010 (Figure 12).

Analysis of this moderate ICME event confirms the predominance of mechanical control, where dynamic pressure (P_d) and density (N) drive the initial compression of the Earth's magnetopause. In this case of moderate ICME storms, variations in B precede those in R_o and significantly influence them. Still, the response of R_o to these constraints only reaches maturity after a 30-minute lag, as in the case of the minor storms 1 and 2 studied. This corresponds to the time required for the global MHD reorganisation of the magnetotail and the stabilisation of the response of the subsolar position (R_o) of the Earth's magnetopause [37]. Although it exhibits Granger causality here, its influence on amplitude remains modest ($r \approx 0.23$), confirming that reconnection coupling, although effective, remains secondary to the dominant mechanical compression processes.

Comparative cross-correlation analysis: moderate CME storms. After analysing Case 1, a comparative study was conducted with Cases 2 and 3 (Figure 13). This combined approach allows distinguishing the predictive coupling delay (Granger) from the maximum response time (R_o) for each solar wind parameter.

Comparative analysis of moderate ICME storms reveals a stable temporal hierarchy: variations in plasma kinetic parameters (P_d, N) precede and significantly influence those of R_o, with R_o exhibiting an instantaneous response. As for B, in all three cases, its variations precede and influence those of R_o, but R_o's response to these magnetic constraints is heterogeneous. In fact, in the first two moderate storms, R_o reacts immediately to B, with a strong correlation, and in the third case, the maximum effect is delayed (30 min) with a very weak correlation ($r = -0.15$). This shows that the impact of B varies with the ICME's internal structure and is not a reliable or universal indicator of the dynamics in these three cases of moderate conditions. The delay observed in case 3, in agreement with Refs. [37, 39], suggests a slowing of the signal in the inner magnetosphere, where the formation of a magnetic barrier and local processes (FTE) may degrade the direct transmission of magnetic stress.

For B_z, the emergence of reconnection coupling (B_z<0) remains weak, with modest correlations ($r \approx 0.23$ to 0.44) despite significant causality. Although secondary to the dominant plasma compression, this signature is consistent with Refs. [7, 40] and demonstrates that the dynamics of R_o are the result of mechanical effects with a modest contribution from magnetic reconnection at the day-side magnetopause in the case of our three moderate ICME events. Thus, the dynamics of the subsolar position (R_o) are mainly governed by pressure equilibrium, in accordance with the classical model [21].

Case of the intense storm of 23 June 2015. The combined analysis of cross-correlation, Granger causality testing, and bootstrap uncertainties enables characterisation of the temporal response dynamics of (R_o) to fluctuations in solar wind parameters during the strong ICME storm of 22 June 2015 (Figure 14).

Unlike the minor and moderate regimes studied, the strong ICME storm is characterised by an instantaneous, synchronous response of the magnetopause's subsolar position (R_o) to all parameters. The dynamic pressure (P_d) and density (N) drive the compression with a maximum correlation at lag = 0 min (r ≈ -0.73). This synchronism reflects a massive transfer of momentum, forcing an instantaneous readjustment of the pressure equilibrium at the subsolar point.

The salient feature of this regime is the disappearance of the magnetic 'maturation' phases observed previously. The intensity of the interplanetary magnetic field (B) exerts a significant influence with a maximum effect on R_o at the immediate (r ≈ −0.64 at lag = 0 min). This regime marks the disappearance of the magnetic maturation phases and indicates accelerated propagation of a magnetic constraint within a stiffened magnetosphere. In agreement with Refs. [37, 39], this near-zero delay indicates that the magnetosheath, which has become very thin, no longer acts as a barrier, allowing for synchronous summation of magnetic and dynamic pressures. Interplanetary energy is no longer dissipated in the inner magnetosheath but is transmitted entirely to the magnetopause.

Although B_z precedes and influences variations in R_o, its impact remains marginal (r ≈ 0.13). The brevity of B_z's southern incursion prevents sustained erosion, leaving the boundary controlled by the brute force of the plasma. The robustness of this chronology, validated by a tight Bootstrap, demonstrates that under this strong ICME storm, the magnetosphere becomes an ultra-reactive transmission medium. For space weather forecasting, this regime requires integrated forecasting of the solar wind's torque (P_d, N) and magnetic pressure, acting in concert without a consolidation delay.

Comparative cross-correlation analysis: case of strong CMEs. After analysing case 1, a comparative study was conducted with cases 2 and 3 (Figure 15). This combined approach allows distinguishing the predictive coupling delay (Granger) from the magnetopause's maximum response time (R_o) for each solar wind parameter, thereby providing a more detailed view of the dynamics under stress.

Comparative analysis of the three strongest ICME storms in cycle 24 shows an almost instantaneous response of the Earth's magnetopause subsolar position (R_o) to the solar wind's kinetic parameters (P_d, N). Unlike the minor and moderate regimes studied, the intensity of the interplanetary magnetic field (B) here reinforces magnetic pressure compression synchronously, without a maturation phase as already observed in case 1. Although B_z activates reconnection coupling from the first minute, its role remains secondary to the predominance of mechanical compression effects in these three cases of strong ICME storms.

However, event 3 reveals a major discrepancy: while the correlation between R_o and torque (P_d, N) is immediate, Granger causality emerges only after ∼13 min. This temporal decorrelation suggests a particularly thick and turbulent ICME sheath, where high-frequency noise initially masks the predictive relationship. This 13-minute delay reflects the transit time of the turbulent plasma in the magnetosheath or the time required to establish a dynamic equilibrium consistent with the incident flux.

Thus, while the strong regime tends towards an immediate response, the ICME's internal structure can introduce significant delays in stabilisation. For space weather, it is therefore crucial to distinguish between the instantaneous response (as measured by the maximum correlation) and the stable response (establishing physical causality) in the typical cases of strong ICME events studied.

Case study: the extreme storm of 17 March 2015. The combined analysis of cross-correlation, Granger causality testing, and bootstrap uncertainties enables characterisation of the temporal response dynamics of (R_o) to fluctuations in solar wind parameters during the extreme ICME storm of 17 March 2015 (Figure 16).

Analysis of this extreme ICME event in the solar cycle reveals a causal chain in which the dynamics of R_o result from a synergy between mechanical and electromagnetic effects. Contrary to classical pressure equilibrium, the combined action of dynamic pressure (P_d) and an intense, sustained southward B_z component triggers massive erosion of the Earth's magnetopause on the day side. This erosion is amplified by the intensity of B, which maximises reconnection efficiency, reducing the magnetosphere's intrinsic resistance and intensifying compression of the Earth's magnetopause. The total solar wind pressure fully exploits the weakening of the boundary following magnetic reconnection on the day side of the magnetosphere, since variations in B also precede those in R_o and significantly influence them, with the maximum effect occurring immediately.

These results refine the work of Refs. [25, 34]: whereas they describe an overall weakening, our study, using the Granger test, shows that electromagnetic coupling is instantaneous in this extreme case. Our results validate the structures of the Refs. [35, 41] models, which introduce the IMF B intensity into their formulations of R_o. This detailed analysis enables distinguishing the triggering of reconnection from the extreme compression phase, a crucial parameter for space weather during typical extreme ICME events.

4. Conclusion

This study demonstrates that the dynamics of the subsolar magnetopause position R_o are governed by a regime transition that depends on the intensity of ICME storms. The first part of the study reveals that the mechanisms controlling the dynamics of R_o vary according to the intensity and phase of these ICME storms. In the case of a minor and moderate ICME storm, R_o is driven almost exclusively by P_d. However, in the case of strong and extreme ICME storms, a shift to a synergistic regime occurs, where magnetic reconnection (B_z<0) in the

strong case or magnetopause erosion in the extreme case becomes as decisive as the mechanical effects of the solar wind in dictating variations in R_o. The analysis shows that crossing the geosynchronous orbit (< 6.6 R_e) is an exclusive signature of the main phase of the strong storm of 22 June 2015, as well as of the initial and main phases of the extreme storm of 17 March 2015. As for the second part of the study, extending the four ICME storms to 10 storms and applying autocorrelation correction by adjusting p-values, the study confirms that high correlations between P_d and N and R_o are signatures of physical causality. For P_d, the relationship remains mostly linear across the minor-to-strong events studied; the use of a second-order polynomial is often counterproductive, leading to overfitting, and this contrast fades in favour of convergence towards non-linearity in the case of the extreme ICME storm studied. Conversely, for B_z, the second-order polynomial model better explains the variance (R^2) in almost all 10 cases, while often dominating in terms of stability and accuracy, suggesting that the response of R_o to magnetic reconnection or erosion is more complex than its response to the mechanical effects of the solar wind. The Bootstrap correction for temporal uncertainty in lags provided final proof of the processes' stability. It showed that in almost all ten cases of the events studied, variations in P_d, N and B precede R_o by 1 to 3 minutes and significantly influence it. The influence of B_z is only activated in moderate cases and becomes significant in extreme cases. The constraint of P_d and N on R_o is maximum at lag = 0 min in all events. On the other hand, the response of R_o to the constraint imposed by B and B_z depends on the intensity of the storm and the internal structure of the responsible ICMEs (sheath zones or ejecta bodies). In fact, a 30-minute delay in response is observed for the low-intensity storms studied, whereas an instantaneous response (lag = 0 min) is observed for strong to extreme storms. These results require a revision of the typical prediction models of Shue *et al.* [5] in favour of saturated dynamic formulations that incorporate adaptive weighting of the total interplanetary magnetic field (B) and a persistence factor for B_z. Furthermore, the evidence of compression anomalies prior to the shock highlights the importance of magnetosphere preconditioning, which can alter its vulnerability to the impact of the ICME. The exceptional expansion of the magnetopause in the main phase to 13.5 Re during the moderate ICME storm of August 2010, following a rarefaction of plasma, highlights a relaxation capacity of the magnetopause that is significantly greater than its nominal equilibrium position. These elements justify further investigation using a larger sample of events to better constrain these processes.

Data availability

The geomagnetic storms induced by CMEs during solar cycle 24 presented in Table 2 were obtained using the catalogue of near-Earth interplanetary coronal mass ejections since January 1996, compiled by Ian Richardson and Hilary Cane, via the website: www.srl.caltech.edu/ACE/ASC/DATA/level3/icmetable2.htm. The dates of sudden starts of geomagnetic storms (SSC) on the ISGI website: http://isgi.unistra.fr/data_download.php and information on coronal mass ejections (CMEs) (speed, nature, etc.) available since 1996 on the CDAW website: http://cdaw.gsfc.nasa.gov/CME_list were also consulted. To model the subsolar position (R_o) and the magnetopause, we used solar wind parameters from the OMNI database (https://omniweb.gsfc.nasa.gov/form/dx1.html). Data relating to the intensity of the interplanetary magnetic field (B), its southern component (B_z), plasma density (N) and dynamic pressure (P_d) were extracted with a temporal resolution of one (01) minute. This high resolution is essential for capturing rapid variations in the solar wind.

References

[1] J. E. Borovsky & M. H. Denton, "Differences between CME-driven storms and CIR-driven storms", Journal of Geophysical Research **111** (2006) 2005JA011447. https://doi.org/10.1029/2005JA011447.

[2] N. Gopalswamy, S. Yashiro & S. Akiyama, Coronal mass ejections and space weather due to extreme events, Proceedings of the ILWS Workshop, Goa, India, 2006, pp. 79. https://cdaw.gsfc.nasa.gov/publications/ilws_goa2006/079_Gopalswamy.pdf.

[3] Y. D. Liu, H. Hu, R. Wang, Z. Yang, B. Zhu, Y. A. Liu, J. G. Luhmann & J. D. Richardson, "Plasma and magnetic field characteristics of solar coronal mass ejections in relation to geomagnetic storm intensity and variability", The Astrophysical Journal **809** (2015) L34. https://doi.org/10.1088/2041-8205/809/2/L34.

[4] J.-H. Shue, J. K. Chao, H. C. Fu, C. T. Russell, P. Song, K. K. Khurana & H. J. Singer, "A new functional form to study the solar wind control of the magnetopause size and shape", Journal of Geophysical Research: Space Physics **102** (1997) 9497. https://doi.org/10.1029/97JA00196.

[5] J.-H. Shue, P. Song, C. T. Russell, J. T. Steinberg, J. K. Chao, G. Zastenker, O. L. Vaisberg, S. Kokubun, H. J. Singer, T. R. Detman & H. Kawano, "Magnetopause location under extreme solar wind conditions", Journal of Geophysical Research: Space Physics **103** (1998) 17691. https://doi.org/10.1029/98JA01103.

[6] J.-H. Shue, Y. Kamide, R. D. Elphinstone & N. Nishitani, "Intense growth phase events of substorms", Journal of Geophysical Research: Space Physics **105** (2000) 5357. https://doi.org/10.1029/1999JA900454.

[7] R. E. F. Bonde, R. E. Lopez & J. Y. Wang, "The effect of IMF fluctuations on the subsolar magnetopause position: a study using a global MHD model", Journal of Geophysical Research: Space Physics **123** (2018) 2598. https://doi.org/10.1002/2018JA025203.

[8] A. A. Samsonov, Y. V. Bogdanova, G. Branduardi-Raymont, J. Safrankova, Z. Nemecek & J.-S. Park, "Long-term variations in solar wind parameters, magnetopause location, and geomagnetic activity over the last five solar cycles", Journal of Geophysical Research: Space Physics **124** (2019) 4049. https://doi.org/10.1029/2018JA026355.

[9] N. Grimmich, A. Pöppelwerth, M. O. Archer, D. G. Sibeck, F. Plaschke, W. Mo, V. Toy-Edens, D. L. Turner, H. Kim & R. Nakamura, "Investigation of the occurrence of significant deviations in the magnetopause location: solar-wind and foreshock effects", Annales Geophysicae **43** (2025) 151. https://doi.org/10.5194/angeo-43-151-2025.

[10] D. G. Sibeck, "Demarcating the magnetopause boundary", Reviews of Geophysics **33** (1995) 651. https://doi.org/10.1029/95RG00285.

[11] T. Iyemori, "Storm-time magnetospheric currents inferred from mid-latitude geomagnetic field variations", Journal of Geomagnetism and Geoelectricity **42** (1990) 1249. https://doi.org/10.5636/jgg.42.1249.

[12] W. D. Gonzalez, J. A. Joselyn, Y. Kamide, H. W. Kroehl, G. Rostoker, B. T. Tsurutani & V. M. Vasyliunas, "What is a geomagnetic storm?", Journal of Geophysical Research: Space Physics **99** (1994) 5771. https://doi.org/10.1029/93JA02867.

[13] C. S. Bretherton, M. Widmann, V. P. Dymnikov, J. M. Wallace & I. Bladé, "The effective number of spatial degrees of freedom of a time-varying field" (1999). https://journals.ametsoc.org/view/journals/clim/12/7/1520-0442_1999_012_1990_tenosd_2.0.co_2.xml.

[14] D. A. Dickey & W. A. Fuller, "Distribution of the estimators for autoregressive time series with a unit root", Journal of the American Statis-

tical Association **74** (1979) 427. https://doi.org/10.1080/01621459.1979.10482531.

[15] C. W. J. Granger, "Investigating causal relations by econometric models and cross-spectral methods", Econometrica **37** (1969) 424. https://doi.org/10.2307/1912791.

[16] S. Iyer & A. Mahajan, "Granger causality analysis of deviation in total electron content during geomagnetic storms in the equatorial region", Journal of Engineering and Applied Science **68** (2021) 4. https://doi.org/10.1186/s44147-021-00007-x.

[17] D. N. Politis & J. P. Romano, "The stationary bootstrap", Journal of the American Statistical Association **89** (1994) 1303. https://doi.org/10.1080/01621459.1994.10476870.

[18] A. Hatemi-J, "Asymmetric causality tests with an application", Empirical Economics **43** (2012) 447. https://doi.org/10.1007/s00181-011-0484-x.

[19] J. R. Spreiter & S. S. Stahara, "Magnetohydrodynamic and gasdynamic theories for planetary bow waves", in *Collisionless Shocks in the Heliosphere: Reviews of Current Research*, American Geophysical Union (AGU), 1985, pp. 85–107. https://doi.org/10.1029/GM035p0085.

[20] J. De Keyser, M. Roth, M. W. Dunlop, H. Rème, C. J. Owen & G. Paschmann, "Empirical reconstruction and long-duration tracking of the magnetospheric boundary in single- and multi-spacecraft contexts", Annales Geophysicae **23** (2005) 1355. https://doi.org/10.5194/angeo-23-1355-2005.

[21] S. Chapman & V. C. A. Ferraro, "A new theory of magnetic storms", Terrestrial Magnetism and Atmospheric Electricity **36** (1931) 171. https://doi.org/10.1029/TE036i003p00171.

[22] J. R. Spreiter, A. Summers & A. Alksne, "Hydromagnetic flow around the magnetosphere", Planetary and Space Science **14** (1966) 223. https://doi.org/10.1016/0032-0633(66)90124-3.

[23] M. H. Farris, S. M. Petrinec & C. T. Russell, "The thickness of the magnetosheath: Constraints on the polytropic index", Geophysical Research Letters **18** (1991) 1821. https://doi.org/10.1029/91GL02090.

[24] M. P. Aubry, C. T. Russell & M. G. Kivelson, "Inward motion of the magnetopause before a substorm", Journal of Geophysical Research **75** (1970) 7018. https://doi.org/10.1029/JA075i034p07018.

[25] Y. P. Maltsev, A. A. Arykov, E. G. Belova, B. B. Gvozdevsky & V. V. Safargaleev, "Magnetic flux redistribution in the storm time magnetosphere", Journal of Geophysical Research: Space Physics **101** (1996) 7697. https://doi.org/10.1029/95JA03709.

[26] Y. P. Maltsev & W. B. Lyatsky, "Field-aligned currents and erosion dayside magnetosphere", Sciences planétaires et spatiales **23** (1975) 1257. https://doi.org/10.1016/0032-0633(75)90149-X.

[27] D. G. Sibeck, R. E. Lopez & E. C. Roelof, "Solar wind control of the magnetopause shape, location, and motion", Journal of Geophysical Research: Space Physics **96** (1991) 5489. https://doi.org/10.1029/90JA02464.

[28] P. M. Dredger, R. E. Lopez, Y. M. Collado-Vega, S. Khurana & L. M. Rastaetter, "Investigating potential causes for the prediction of spurious magnetopause crossings at geosynchronous orbit in MHD simulations", Space Weather **21** (2023) e2022SW003266. https://doi.org/10.1029/2022SW003266.

[29] J. W. Dungey, "Interplanetary magnetic field and the auroral zones", Physical Review Letters **6** (1961) 47. https://doi.org/10.1103/PhysRevLett.6.47.

[30] R. E. Holzer & J. A. Slavin, "Magnetic flux transfer associated with expansions and contractions of the dayside magnetosphere", Journal of Geophysical Research: Space Physics **83** (1978) 3831. https://doi.org/10.1029/JA083iA08p03831.

[31] J. Raeder, Y. L. Wang, T. J. Fuller-Rowell & H. J. Singer, "Global simulation of magnetospheric space weather effects of the Bastille Day storm", Physique solaire **204** (2001) 323. https://doi.org/10.1023/A:1014228230714.

[32] D. Herrera, V. F. Maget & A. Sicard-Piet, "Characterizing magnetopause shadowing effects in the outer electron radiation belt during geomagnetic storms", Journal of Geophysical Research: Space Physics **121** (2016) 9517. https://doi.org/10.1002/2016JA022825.

[33] G. Le, H. Lühr, B. J. Anderson, R. J. Strangeway, C. T. Russell, H. Singer, J. A. Slavin, Y. Zhang, T. Huang, K. Bromund, P. J. Chi, G. Lu, D. Fischer, E. L. Kepko, H. K. Leinweber, W. Magnes, R. Nakamura, F. Plaschke, J. Park, J. Rauberg, C. Stolle & R. B. Torbert, "Magnetopause erosion during the 17 March 2015 magnetic storm: Combined field-aligned currents, auroral oval, and magnetopause observations", Geophysical Research Letters **43** (2016) 2396. https://doi.org/10.1002/2016GL068257.

[34] H. Kim, H. K. Connor, Y. Zou, J. Park, R. Nakamura & K. McWilliams, "Relation between magnetopause position and reconnection rate under quasi-steady solar wind dynamic pressure", Earth, Planets and Space **76** (2024) 165. https://doi.org/10.1186/s40623-024-02101-9.

[35] R. L. Lin, X. X. Zhang, S. Q. Liu, Y. L. Wang & J. C. Gong, "A three-dimensional asymmetric magnetopause model", Journal of Geophysical Research: Space Physics **115** (2010). https://doi.org/10.1029/2009JA014235.

[36] J. Wang, Z. Guo, Y. S. Ge, A. Du, C. Huang & P. Qin, "The responses of the earth's magnetopause and bow shock to the IMF Bz and the solar wind dynamic pressure: A parametric study using the AMR-CESE-MHD model", Journal of Space Weather and Space Climate **8** (2018) A41. https://doi.org/10.1051/swsc/2018030.

[37] A. A. Samsonov, D. G. Sibeck, N. P. Dmitrieva & V. S. Semenov, "What happens before a southward IMF turning reaches the magnetopause?", Geophysical Research Letters **44** (2017) 9159. https://doi.org/10.1002/2017GL075020.

[38] M. Wiltberger, R. E. Lopez & J. G. Lyon, "Magnetopause erosion: A global view from MHD simulation", Journal of Geophysical Research: Space Physics **108** (2003) 2002JA009564. https://doi.org/10.1029/2002JA009564.

[39] M. P. Freeman & D. J. Southwood, "The correlation of variations in the IMF with magnetosheath field variations", Advances in Space Research **8** (1988) 217. https://doi.org/10.1016/0273-1177(88)90134-2.

[40] R. E. Lopez, R. Bruntz, E. J. Mitchell, M. Wiltberger, J. G. Lyon & V. G. Merkin, "Role of magnetosheath force balance in regulating the dayside reconnection potential", Journal of Geophysical Research: Space Physics **115** (2010). https://doi.org/10.1029/2009JA014597.

[41] Z.-Q. Liu, J. Y. Lu, C. Wang, K. Kabin, J. S. Zhao, M. Wang, J. P. Han, J. Y. Wang & M. X. Zhao, "A three-dimensional high Mach number asymmetric magnetopause model from global MHD simulation", Journal of Geophysical Research: Space Physics **120** (2015) 5645. https://doi.org/10.1002/2014JA020961.